1-1-2017

Disrupted murine gut-to-human liver signaling alters bile acid homeostasis in humanized mouse liver models

Edwin C.Y. Chow
University of Toronto

Holly P. Quach
University of Toronto

Yueping Zhang
Bristol-Myers Squibb

Jason Z.Y. Wang
University of Toronto

David C. Evans
Janssen Research & Development

See next page for additional authors

1521-0103/360/1/174–191$25.00
THE JOURNAL OF PHARMACOLOGY AND EXPERIMENTAL THERAPEUTICS

http://dx.doi.org/10.1124/jpet.116.236935
J Pharmacol Exp Ther 360:174–191, January 2017

The Journal of PHARMACOLOGY And Experimental Therapeutics

Disrupted Murine Gut–to–Human Liver Signaling Alters Bile Acid Homeostasis in Humanized Mouse Liver Models[S]

Edwin C. Y. Chow, Holly P. Quach, Yueping Zhang, Jason Z. Y. Wang, David C. Evans, Albert P. Li, Jose Silva, Rommel G. Tirona, Yurong Lai, and K. Sandy Pang

Department of Pharmaceutical Sciences, Leslie Dan Faculty of Pharmacy, University of Toronto, Toronto, Ontario, Canada (E.C.Y.C., H.P.Q., J.Z.Y.W., K.S.P.); Bristol Myers Squibb, Pharmaceutical Candidate Optimization Department, Princeton, New Jersey (Y.Z., Y.L.); Pharmacokinetics, Dynamics, and Metabolism, Janssen Research and Development, LLC, Spring House, Pennsylvania (D.C.E., J.S.); In Vitro ADMET Laboratories, Columbia, Maryland (A.P.L.); Department of Physiology and Pharmacology and Medicine, Schulich School of Medicine and Dentistry, University of Western Ontario, London, Ontario, Canada (R.G.T.)

Received August 1, 2016; accepted October 25, 2016

ABSTRACT

The humanized liver mouse model is being exploited increasingly for human drug metabolism studies. However, its model stability, intercommunication between human hepatocytes and mouse nonparenchymal cells in liver and murine intestine, and changes in extrahepatic transporter and enzyme expressions have not been investigated. We examined these issues in FRGN [fumarylacetoacetate hydrolase (*Fah*−/−), recombination activating gene 2 (*Rag2*−/−), and interleukin 2 receptor subunit gamma (*IL-2rg* −/−) triple knockout] on nonobese diabetic (NOD) background] and chimeric mice: mFRGN and hFRGN (repopulated with mouse or human hepatocytes, respectively). hFRGN mice showed markedly higher levels of liver cholesterol, biliary bilirubin, and bile acids (liver, bile, and plasma; mainly human forms, but also murine bile acids) but lower transforming growth factor beta receptor 2 (TGFBR2) mRNA expression levels (10%) in human hepatocytes and other proliferative markers in mouse nonparenchymal cells (Tgf-β1) and cholangiocytes [plasma membrane–bound, G protein-coupled receptor for bile acids (Tgr5)], suggestive of irregular regeneration processes in hFRGN livers. Changes in gene expression in murine intestine, kidney, and brain of hFRGN mice, in particular, induction of intestinal farnesoid X receptor (Fxr) genes: fibroblast growth factor 15 (Fgf15), mouse ileal bile acid binding protein (Ibabp), small heterodimer partner (Shp), and the organic solute transporter alpha (Ostα), were observed. Proteomics revealed persistence of remnant murine proteins (cyotchrome P450 7α-hydroxylase (Cyp7a1) and other enzymes and transporters) in hFRGN livers and suggest the likelihood of mouse activity. When compared with normal human liver tissue, hFRGN livers showed lower SHP mRNA and higher CYP7A1 (300%) protein expression, consequences of tβ- and tα-muricholic acid–mediated inhibition of the FXR-SHP cascade and miscommunication between intestinal Fgf15 and human liver fibroblast growth factor receptor 4 (FGFR4), as confirmed by the unchanged hepatic pERK/total ERK ratio. Dysregulation of hepatocyte proliferation and bile acid homeostasis in hFRGN livers led to hepatotoxicity, gallbladder distension, liver deformity, and other extrahepatic changes, making questionable the use of the preparation for drug metabolism studies.

Introduction

Humanized (h-chimeric) liver mouse models are preclinical tools that are used for the prediction of human drug metabolism (Sanoh and Ohta, 2014). Unlike the transgenic mouse models, h-chimeric liver mouse models that are repopulated with human hepatocytes consist of the full complementary array of human liver genes. The triple genetic knockout FRGN mouse model [fumarylacetoacetate hydroxylase (*Fah*−/−), recombination-activating gene 2 (*Rag2*−/−), and interlukin 2 receptor subunit gamma (*Il2rg*−/−) triple knockout] on nonobese diabetic strain (NOD) background] is one of these models in which absence of the *Fah* gene results in liver accumulation of the toxic metabolite, fumarylacetoacetate, which induces hepatic injury and allows for repopulation of foreign hepatocytes (Azuma et al., 2007). Toxicity is alleviated when these mice are given daily supplements of 2-(2-nitro-4-trifluoro-methylbenzoyl)-1,3-cyclohexanedione (NTBC), which blocks fumarylacetoacetate production and allows for a controllable environment in which a series of hepatocyte implantations for successful engraftment can be achieved.

The h-chimeric liver mouse models are being used increasingly for human drug metabolism studies (Katoh et al., 2004; Tateno et al., 2004; Katoh et al., 2005a, b, 2007; Ohtsuki et al., 2014) and have provided preliminary insights on human metabolite formation in vivo (Liu et al., 2011; Sanoh et al., 2012; Bateman et al., 2014; Kitamura and Sugihara, 2014). These mice respond to selective induction of ligands for human-specific nuclear receptors (Katoh et al., 2005a; Emoto et al., 2008; Sanoh and Ohta, 2014). In addition, h-chimeric liver mouse models have been used to study preclinical drug-drug interactions (Jaiswal et al., 2014) and drug-induced liver injury stemming from troglitazone (Barnes et al., 2014; Samuelsson et al., 2014), bosentan (Xu et al., 2015), and fialuridine (Xu et al., 2014), and have provided an essential in vivo safety testing tool for potential human toxic

Funding was provided by Janssen Pharmaceutical Inc., Spring House, PA.
dx.doi.org/10.1124/jpet.116.236935.
[S] This article has supplemental material available at jpet.aspetjournals.org.

metabolites (Strom et al., 2010; Cohen, 2014; Kitamura and Sugihara, 2014; Xu et al., 2015).

A sound comparison of the pharmacokinetic and metabolic data with h-chimeric liver mouse models is dependent on the premise that the model is stable, with little or no change in transporters and enzymes in extrahepatic tissues that are also under regulation by nuclear receptors (Makishima, 2005). The farnesoid X receptor (FXR), liver X receptor (LXR), pregnane/steroid X receptor (PXR/SXR), and constitutive androstane receptor (CAR) are major nuclear receptors that are responsible for the regulation of transporters and enzymes in the body. Although these nuclear receptors in human and other species share common targets, species difference in nuclear receptor activation exists, and this will pose as a major concern in ligand-specific nuclear receptor activation (Chiang et al., 2001; Handschin and Meyer, 2003; Katoh et al., 2005a; Sayin et al., 2013) in the h-chimeric liver model.

We recently observed remarkable physiologic and metabolic zonation differences between hFRGN and FRGN mouse livers. Notably, hFRGN livers contain remnant mouse transporters and enzymes that are present at similar or even higher levels than those in FRGN livers (Chow et al., 2016). One possible explanation is that changes in intrinsic factors such as hormone and bile acid production, as regulated by intestinal and hepatic nuclear receptors, will lead to changes in liver transporter and enzyme levels. At high bile acid concentrations, human cytochrome P450 7α-hydroxylase (CYP7A1), the rate-limiting enzyme for bile acid synthesis, is negatively regulated by the FXR–small heterodimer partner (SHP) cascade (Chiang, 2003, 2009) and by the fibroblast growth factor 15/19 (mouse Fgf15, human ortholog FGF19), a hormone that is secreted by the ileum and binds to liver fibroblast growth factor receptor 4 (FGFR4) to activate the *c*-Fos pathway for repressing CYP7A1 in a negative feedback mechanism (Inagaki et al., 2005; Lin et al., 2007). In h-chimeric livers, CYP7A1 and human bile acid levels were observed to be dramatically elevated, but the condition was corrected upon administration of exogenous FGF19 or transfection of FGF19 gene in h-chimeric mice (Ellis et al., 2013; Naugler et al., 2015).

To fully understand bile acid dysregulation in these h-chimeric mice, we examined individual mouse and human bile acid species by liquid chromatography coupled with tandem mass spectrometry (LC-MS/MS) and employed proteomics to quantify changes in mouse and human CYP7A1 and other proteins. We included mFRGN mice (FRGN liver with foreign mouse hepatocyte repopulation) in this study as another control to ensure that observations were independent of the diet/housing and surgical manipulation (Chow et al., 2016). Because the status of each organ/tissue could potentially impact the functionality of others (Naud et al., 2007, 2008), we appraised key biologic and physiologic parameters, and human and mouse gene expression in liver, including proliferative genes in nonparenchymal cells and in extrahepatic tissues to fully understand the interorgan communication between human and mouse organs in hFRGN mice.

Methods

Materials. Cholic acid (CA), chenodeoxycholic acid (CDCA), deoxycholic acid (DCA), lithocholic acid (LCA), ursodeoxycholic acid (UDCA), taurocholic acid (tCA) sodium salt hydrate, taurochenodeoxycholic acid (tCDCA) sodium salt, taurodeoxycholic acid (tDCA) sodium salt, and taurolithocholic acid (tLCA) sodium salt were obtained from Sigma Aldrich Canada (Oakville, ON). Muricholic acid (MCA), α-, β-, and ω-muricholic acids (α-, β-, and ω-MCA), tauro-α-, tauro-β- and tauro-ω-muricholic acid (tα-, tβ-, and tω-MCA) sodium salts, and tauroursodeoxycholic acid (tUDCA) sodium salt were obtained from Steraloids (Newport, RI). Glycocholic acid (gCA), glycochenodeoxycholic acid (gCDCA), glycodeoxycholic acid (gDCA), glycolithocholic acid (gLCA), and glycoursodeoxycholic acid (gUDCA) were kind gifts from Dr. Alan F. Hofmann (University of California, San Diego). Cholic-2,2,4,4-d_4 acid (CA-d_4), chenodeoxycholic-2,2,4,4-d_4 acid (CDCA-d_4), deoxycholic-2,2,4,4-d_4 acid (DCA-d_4), and lithocholic-2,2,4,4-d_4 acid (LCA-d_4) were purchased from C/D/N Isotopes (Pointe-Claire, QC).

Mice and Housing Conditions. Male FRGN, mFRGN [FRGN livers repopulated with pooled mouse hepatocytes of the Rosa (129S7) mouse strain], and hFRGN [FRGN livers with human hepatocyte repopulation] mice (4–6 months old from three different human donors of ages 5, 7, and 17, Table 1) were supplied by Yecuris Corporation (Tualatin, OR). All hFRGN livers were >80% human repopulated, as stated by Yecuris. The housing and diet conditions of FRGN, mFRGN, and hFRGN mice have been previously described in detail by Chow et al. (2016). All animal studies were performed in accordance to approved animal protocols at the University of Toronto.

ABBREVIATIONS: α-, β-, and ω-MCA, α-, β-, and ω-muricholic acids; ACN, acetonitrile; ALT, alanine aminotransferase; Baat/BAAT, murine/human bile acid CoA/amino acid *N*-acyltransferase; Bcrp/BCRP, murine/human breast cancer resistance protein; Bsep/BSEP, murine/human bile salt export pump; CA, cholic acid; Car/CAR, murine/human constitutive androstane receptor; CDCA, chenodeoxycholic acid; Cyp7a1/CYP7A1, murine/human cytochrome P450 7α-hydroxylase; DCA, deoxycholic acid; ddH_2O, double-distilled water; ELISA, enzyme-linked immunosorbent assay; Fgf15/FGF19, rodent or human fibroblast growth factor 15/19; Fgfr4/FGFR4, murine/human fibroblast growth factor receptor 4; FRGN, triple knockout of *Fah, Rag2, and Il2rg* genes on the nonobese diabetic strain background; Fxr/FXR, murine/human farnesoid X receptor; gCA, glycocholic acid; gCDCA, glycochenodeoxycholic acid; gDCA, glycodeoxycholic acid; gLCA, glycolithocholic acid; gUDCA, glycoursodeoxycholic acid; GAPDH, human glyceraldehyde-3-phosphate dehydrogenase; Gsta/GSTA, murine/human glutathione *S*-transferase; hFRGN or h-chimeric, humanized liver mouse or FRGN mouse with human-hepatocyte repopulated liver; Hnf-4α/HNF-4α, murine/human hepatocyte nuclear factor 4 alpha; LC-MS/MS, liquid chromatography–tandem mass spectrometry; LCA, lithocholic acid; Lrh-1/LRH-1, murine/human liver receptor homolog 1; Lxrα/LXR, murine/human liver X receptor alpha; MCA, muricholic acid; Mdr1a/MDR1, murine/human multidrug resistance protein 1; MeOH, methanol; mFRGN, FRGN mouse with foreign mouse-hepatocyte [Rosa (129S7) strain] repopulated liver; Mrp/MRP, murine/human multidrug resistance–associated protein; MRM, multiple reaction monitoring; NH_4OH, ammonium hydroxide; NTBC, nitisinone or 2-(2-nitro-4-trifluoromethylbenzoyl)-1,3-cyclohexanedione; Ntcp/NTCP, murine/human sodium-dependent taurocholate–cotransporting polypeptide; Oat, mouse organic anion transporter; Oatp/OATP, murine/human organic anion–transporting polypeptide; Ost/OST, murine/human organic solute transporter (α or β); P-gp, P-glycoprotein; Pxr/PXR/SXR, murine/human pregnane X receptor, also known as steroid X receptor; Shp/SHP, murine/human small heterodimer partner; tα-, tβ-, and tω-MCA, tauro-α-, tauro-β-, tauro-ω-muricholic acid; tCA, taurocholic acid; tCDCA, taurochenodeoxycholic acid; tDCA, taurodeoxycholic acid; TGF-β1/TGF-β, transforming growth factor beta; TGFBR2, transforming growth factor beta receptor 2; Tgr5, plasma membrane–bound, G protein-coupled receptor for bile acids; tLCA, taurolithocholic acid; tUDCA, tauroursodeoxycholic acid; UDCA, ursodeoxycholic acid; Ugt/UGT, murine/human UDP-glucuronosyltransferases

TABLE 1
hFRGN human donor and human liver tissue information
All hFRGN livers were >80% human repopulated, as indicated by Yecuris. Human liver tissues were from In Vitro ADMET, Columbia, MD

Mouse ID	Human Donors ID	Donor Information	Human Albumin	Experiments
			mg/ml	
hFRGN3	HHF07007	Female, Caucasian, 7 years old	7.2	Liver mRNA and protein
hFRGN4	HHF07007	Female, Caucasian, 7 years old	4.9	Liver mRNA and protein
hFRGN5	HHF07007	Female, Caucasian, 7 years old	4.6	Liver mRNA and protein
hFRGN6	HHF07007	Female, Caucasian, 7 years old	5.3	mRNA and protein; bile acid LC-MS/MS
hFRGN7	HHF07007	Female, Caucasian, 7 years old	15.5	mRNA and protein; bile acid LC-MS/MS
hFRGN10	HHM05010	Male, Caucasian, 5 years old	4.8	Liver mRNA and protein
hFRGN11	HHM05010	Male, Caucasian, 5 years old	4.0	mRNA and protein; bile acid LC-MS/MS
hFRGN12	HHM05010	Male, Caucasian, 5 years old	4.0	Histology
hFRGN13	HHF17006	Female, Caucasian, 17 years old	6.3	mRNA and protein; bile acid LC-MS/MS
hFRGN14	HHF17006	Female, Caucasian, 17 years old	7.1	mRNA and protein; bile acid LC-MS/MS
hFRGN15	HHF17007	Female, Caucasian, 7 years old	5.7	mRNA and protein; bile acid LC-MS/MS
hFRGN16	HHF17007	Female, Caucasian, 7 years old	4.4	mRNA and protein; bile acid LC-MS/MS
hFRGN26	HHF17006	Female, Caucasian, 17 years old	5.2	Bile acid pool size LC-MS/MS
hFRGN27	HHF17006	Female, Caucasian, 17 years old	3.9	Bile acid pool size LC-MS/MS
hFRGN28	HHF17006	Female, Caucasian, 17 years old	3.5	Bile acid pool size LC-MS/MS
hFRGN29	HHF17006	Female, Caucasian, 17 years old	3.5	Bile acid pool size LC-MS/MS
Human liver 1	H1016	Female, Hispanic, 64 years old	NA	Liver mRNA
Human liver 2	H1028	Male, Hispanic, 43 years old	NA	Liver mRNA
Human liver 3	H1041	Male, Caucasian, 53 Years old	NA	Liver mRNA
Human liver 4	H1047	Male, Hispanic, 44 years old	NA	Liver mRNA
Human liver 5	H1057	Female, Caucasian, 33 years old	NA	Liver mRNA
Human liver 6	H1072	Female, Caucasian, 40 years old	NA	Liver mRNA

NA, not available.

Biologic Assays. Plasma alanine aminotransaminase (ALT) from fresh plasma samples were immediately quantified by the ALT kit (Bioquant, Nashville, TN), and plasma and liver cholesterol and liver triglyceride levels were measured using total cholesterol (Wako Diagnostics, Richmond, VA, and Thermo Scientific, Rockford, IL, respectively) and triglyceride (Thermo Scientific) kits, as previously described by Chow et al. (2014). Total and conjugated bilirubin in bile were assayed by the bilirubin assay kit (SigmaAldrich Canada) after a 15-fold dilution with saline.

Oil Red O Staining. After flushing of the mouse liver with ice-cold saline, livers were fixed with 10% formalin overnight for hematoxylin and eosin staining, followed by Oil Red O staining, as performed by the Toronto Centre for Phenogenomics (Toronto, ON).

Bile Acid Quantification from Bile, Plasma, Liver, and Pool Size Using LC-MS/MS. The bile ducts of FRGN, mFRGN, and hFRGN mice were cannulated under anesthesia after gallbladder ligation with PE10 tubing for continuous bile collection in vivo for 10–20 minutes. Blood was then collected by cardiac puncture with a heparinized needle/syringe, and the sample was centrifuged to obtain plasma. Ice-cold saline was pushed through the vena cava to flush blood out of tissues. Enterocytes from intestine [duodenal, proximal jejunal, and ileal segments, with enterocytes removed by a scraper as described (Chow et al., 2014)], kidney, liver, and brain were collected, cut into pieces, snap-frozen in liquid nitrogen, and stored at –80°C for future analyses.

The detailed description of sample preparation for bile acids in plasma, bile, and liver tissue, and the bile acid pool size study was as follows. For bile acid sample preparation, the aliquot was first diluted 100-fold with double-distilled (dd)H_2O, followed by addition of 20 μl methanol (MeOH)/dd$H_2$0 (50:50 v/v) containing a mixture of the internal standards [1 μg/ml of CDCA-d_4, CA-d_4, DCA-d_4, and LCA-d_4 (C/D/N Isotopes, Pointe-Claire, Canada)]. The resultant mixture was added to the preconditioned solid-phase extraction (SPE) (Strata-X; Phenomenex, Torrance, CA) column (2 ml MeOH, followed by 2 ml ddH_2O). The column was then eluted with 2 ml ddH_2O for clearing unwanted debris. Outflow collection was initiated upon elution with 4 ml MeOH. The eluent was dried under nitrogen gas, reconstituted with 100 μl MeOH/ddH_2O mixture, vortexed for 1 minute, and centrifuged at 12,000*g* for 10 minutes at room temperature prior to injection. For plasma sample preparation, 100 μl of sample was added to 20 μl of the internal standard mixture and precipitated with 1 ml ice-cold acetonitrile (ACN) containing 5% 1 N ammonium hydroxide (NH_4OH). The mixture was vortexed for 1 minute, centrifuged at 12,000*g* for 10 minutes at 4°C, and 1 ml supernatant was pipetted and dried under nitrogen gas. The residue was reconstituted with 100 μl MeOH/ddH_2O mixture, vortexed for 1 minute, and centrifuged at 12,000*g* for 10 minutes at room temperature prior to injection. For liver tissue preparation, the liver was homogenized with ddH_2O (1:2, w/v) on ice. The homogenate (100 μl) was then added with 20 μl of the internal standard mixture and precipitated with 1 ml ice-cold ACN (in 5% 1 N NH_4OH). The mixture was vortexed for 1 minute, centrifuged at 12,000*g* for 10 minutes at 4°C, and 1 ml supernatant was pipetted and dried under nitrogen gas. The residual homogenate mixture was reprecipitated with another 1 ml of ice-cold ACN (in 5% 1 N NH_4OH), vortexed, spun, collected in the same collection tube, and dried under nitrogen gas. The residue was reconstituted with 100 μl MeOH/ddH_2O mixture, vortexed for 1 minute, and centrifuged at 12,000*g* for 10 minutes at room temperature prior to injection.

For preparation of the calibration curves for bile acids in each biologic matrix, blank sample matrix was first prepared. Blank bile (diluted 100-fold with ddH_2O), plasma, and liver homogenates (1:2, w/v with saline) were incubated with charcoal (100 mg/ml final concentration) and the sample was kept shaking overnight at 4°C. The resulting solution was spun at 9000*g* for 10 minutes, and the supernatant was filtered through a 0.45-μm pore size Supor polyethersulfone membrane syringe filter (Pall Life Sciences, Port Washington, NY). When these blank sample matrices were tested for the presence of bile acids with LC-MS/MS, none was found (below limit of quantification). Hence, for standard curves, bile, plasma, and liver homogenate tissue were first stripped of endogenous bile acids, then the appropriate standards were added (0.01–10 μg/ml final concentration for each bile acid species) and processed in the same manner as described above.

Bile Acid Extraction for Bile Acid Pool Size. The bile acid extraction procedure was similar to that previously described by Chow et al. (2014). On the last day of study, mice were fasted for 4 hours (from 9 AM to 1 PM). The intact gallbladder, liver, and intestine were removed together under anesthesia. Tissues were minced into pieces in a beaker containing 50 ml of anhydrous ethanol added with 50 μl of

the internal standards (a mixture of 0.25 mg/ml of CDCA-d_4, CA-d_4, DCA-d_4, and LCA-d_4). The content was boiled at 80°C (ethanol boiling point) for 1 hour, and ethanol was added during the heating/incubation to replace evaporated liquid. After cooling, the extracts were filtered through Whatman filter paper and adjusted to 50 ml with ethanol in a volumetric flask. Some extracts were centrifuged at 10,000*g* for 10 minutes and filtered through an Ultra-free-MC centrifugal filter device containing a 0.22-μm polyvinylidene fluoride (PVDF) membrane (Millipore, Billerica, MA) prior to analysis. Bile acid standards, prepared in different concentrations (0.1–50 μM), were extracted in a similar manner.

LC-MS/MS for Bile Acid Quantification. Extracted samples from bile, plasma, liver homogenate, and bile acid pool size were analyzed by LC-MS/MS using the AB Sciex API 4000 Triple Quad LC/MS instrument (Applied Biosystems/ThermoFisher Scientific, Sunnyvale, CA) with electrospray ionization source in the negative ion mode. Samples (10 μl) were injected and separated by a Kinetex 2.6-μm C18 100A 100 × 4.6-mm column (Phenomenex), with a SecurityGuard precolumn (Phenomenex) at 600 μl/min flow rate. The mobile phase consisted of prefiltered 10 mM ammonium acetate (A) and high-performance liquid chromatography grade ACN (B). A gradient was used over 20 minutes: 0–6 minutes, 35–35% solvent B; 6–14 minutes, 35–58% solvent B; 14–15 minutes, 58–95% solvent B; 15–16.5 minutes, 95–95% solvent B; 16.5–17 minutes, 95–35% solvent B; 17–20 minutes, 35–35% solvent B. MS parameters are listed in Table 2, and a gas temperature of 500°C, ion spray voltage of 3500V, and column ambient temperature were used. Selective ion monitoring was employed to detect the conjugated and unconjugated bile acids. Bile acids were quantified on the basis of area of the peak of the standard, corrected by area of the appropriate deuterated internal standard, in calibration curves (Table 2).

FGF19 in Plasma, Liver, Bile, and Gallbladder. Minced, frozen hFRGN liver tissues were homogenized in phosphate-buffered saline (PBS) (10 mM, pH 7.0; 1:1, w/v) over ice. The resultant homogenate was sonicated with a cell disrupter and then centrifuged at 5000*g* for 5 minutes to provide a supernatant for later analysis. Plasma (diluted 2-fold), liver supernatant (diluted 5-fold), bile (diluted 40-fold), and gallbladder (diluted 5-fold) samples were diluted with PBS and assayed using a human FGF19 ELISA kit (R&D Systems Inc., Minneapolis, MN), following the manufacturer's protocol. We also tried quantifying Fgf15 levels using enzyme-linked immunosorbent assay (ELISA). However, these levels were not reported since the values were considered unreliable (personal communication with Dr. S. A. Kliewer).

Proteomics. Protein expression (Karlgren et al., 2012) was determined by peptide-based LC-MS/MS measurements (Vildhede et al., 2014). Quantification of proteins in hFRGN (n = 9), FRGN (n = 8), and human liver (n = 3) tissues (see Table 1 for donor information) was accomplished by mass spectrometry–based targeted proteomics using validated LC−MS/MS methods, as previously described (Groer et al., 2013).

Tissue was homogenized by a Cellcrusher tissue pulverizer (Schull, Cork, Ireland). The peptide sequence and multiple reaction monitoring (MRM) transition for each peptide and isotopically labeled peptide as internal standard for quantification are listed in Table 3. An isotope-labeled peptide was used as the internal standard for each peptide (Table 3). Protein was determined by the protein bicinchoninic acid kit from Pierce Biotechnology (Rockford, IL). An aliquot of 200 μg membrane protein was digested with Mass Spec Grade Trypsin/Lys-C Mix (Promega, Madison, WI) (Qiu et al., 2013). Membrane fractions were extracted using ProteoExtract Native Membrane Extraction Kit (Calbiochem, San Diego, CA) according to the manufacturer's protocol, and 20 μl of the reconstituted, digested sample was injected into the Shimadzu LC system (LC-30A) (Shimadzu Corp., Kyoto, Japan) coupled with the ABSciex 6500 QTrap equipped with TurboSpray ion source operating at positive-ion mode (Foster City, CA). All chromatographic separations were performed by gradient elution with a Waters Acquity UPLC Peptide BEH C18 130A 1.7-μm 2.1× 150-mm column (Waters Corp, Milford, MA), maintained at 60°C at a flow rate of 300 μl/min. The gradient program started as 10% mobile phase A (0.1% formic acid in water), increased to 30% B (0.1% formic acid in ACN) over 25 minutes, followed by a sharp increase to 90% B in the next 0.5 minutes, then maintained at 90% B for 2 minutes. The gradient was then decreased to 10% B in 0.2 minutes, and held for

TABLE 2
Bile acid standards and parameters for LC-MS/MS

Name	Symbol	m/z	Internal Standard	Declustering Potential	Collision Energy	Cell Exist Potential
				V	*eV*	*V*
Cholic acid	CA	407.3→407.3	CA-d_4	−125	−25	−5
α-Muricholic acid	α-MCA	407.3→407.3	CA-d_4	−125	−25	−5
β-Muricholic acid	β-MCA	407.3→407.3	CA-d_4	−125	−25	−5
ω-Muricholic acid	ω-MCA	407.3→407.3	CA-d_4	−125	−25	−5
Chenodeoxycholic acid	CDCA	391.3→391.3	CDCA-d_4	−130	−25	−5
Deoxycholic acid	DCA	391.3→391.3	DCA-d_4	−130	−25	−5
Muricholic acid	MCA	391.3→391.3	CA-d_4	−130	−25	−5
Ursodeoxycholic acid	UDCA	391.3→391.3	CDCA-d_4	−130	−25	−5
Lithocholic acid	LCA	375.3→375.3	LCA-d_4	−120	−23	−5
Glycocholic acid	G-CA	464.3→73.9	CA-d_4	−85	−74	−5
Glycoursodeoxycholic acid	gUDCA	448.3→73.9	CDCA-d_4	−80	−74	−5
Glycodeoxycholic acid	gDCA	448.3→73.9	CDCA-d_4	−80	−74	−5
Glycochenodeoxycholic acid	gCDCA	448.3→73.9	CDCA-d_4	−80	−74	−5
Glycolithocholic acid	gLCA	432.3→73.9	LCA-d_4	−80	−64	−5
Taurocholic acid	tCA	514.3→79.9	CA-d_4	−120	−120	−5
Tauro-α-muricholic acid	tα-MCA	514.3→79.9	CA-d_4	−120	−120	−5
Tauro-β-muricholic acid	tβ-MCA	514.3→79.9	CA-d_4	−120	−120	−5
Tauro-ω-muricholic acid	tω-MCA	514.3→79.9	CA-d_4	−120	−120	−5
Tauroursodeoxycholic acid	tUDCA	498.3→79.9	CDCA-d_4	−110	−120	−5
Taurochenodeoxycholic acid	tCDCA	498.3→79.9	CDCA-d_4	−110	−120	−5
Taurodeoxycholic acid	tDCA	498.3→79.9	DCA-d_4	−110	−120	−5
Taurolithocholic acid	tLCA	482.3→79.9	LCA-d_4	−130	−120	−5
Cholic-2,2,-4-4-d_4 acid	CA-d_4	411.3→411.3		−125	−25	−5
Deoxycholic-2,2,-4-4-d_4 acid	DCA-d_4	395.3→395.3		−130	−25	−5
Chenodeoxycholic-2,2,-4-4-d_4 acid	CDCA-d_4	395.3→395.3		−130	−25	−5
Lithocholic-2,2,-4-4-d_4 acid	LCA-d_4	379.3→379.3		−120	−23	−5

TABLE 3
Specific peptide sequence for detection of surrogate proteins and MRM conditions

Protein	Species Cross-Reactivity	Peptide Sequence	Q1	Q3	Declustering Potential	Collision Energy	Cell Exist Potential
			m/z	*m/z*	*V*	*eV*	*V*
CYP7A1/Cyp7a1	Human/mouse/rat	LSSASLNIR	480.8	760.4	66	23	32
CYP7A1	Human	AHILNNLDNFK	433.4	523.1	44	15	20
Cyp7a1	Mouse/rat	LFAVQEIK	474.2	616.2	66	23	26
Oatp1b2	Mouse/rat	SVQPELK	400.7	614.3	80	17	26
NTCP/Ntcp	Human/mouse/rat	GIYDGDLK	440.8	710.2	80	17	26
BSEP/Bsep	Human/mouse/rat	STALQLIQR	515.4	657.5	90	25	26
BCRP/Bcrp	Human/mouse/rat	SSLLDVLAAR	522.9	644.3	100	25	26
P-gp	Human/mouse/rat	AGAVAEEVLAAIR	635.3	971.4	95	31	25
MRP2/Mrp2	Human/rat	LTIIPQDPILFSGSLR	885.8	665.5	90	37	25
MRP3/Mrp3	Human	IDGLNVADIGLHDLR	541.6	697.2	90	20	18
MRP4/Mrp4	Human/mouse/rat	APVLFFDR	482.8	697.4	66	28	21

2 minutes. The mass spectrometer ion spray voltage was 5000V, temperature was 450°C, curtain gas was at 40 psi, and ion source gas 1 and ion source gas 2 were at 85 and 60 psi, respectively. Detection was accomplished by mass spectrometry–based targeted proteomics using validated LC−MS/MS methods, as previously described (Groer et al., 2013). Analyses were performed in scheduled multiple reactions monitoring (SMRM) mode. Peak integration and quantification were performed using the Analyst 1.6.2 software (MDS Sciex, Concord, ON). The final protein expression (fmol per μg membrane protein) was calculated upon normalization of the isolated membrane fraction as described by Li et al. (2008), and the accuracy (error) and precision (CV) were <20%. Each sample was analyzed in duplicate (technical repeats).

Quantitative Real-Time Polymerase Chain Reaction. Total mRNA in tissue was isolated with the standard TRIzol extraction procedure and quantified as previously described (Chow et al., 2009, 2014). Specific mouse and human primers were designed in Primer-BLAST (http://www.ncbi.nlm.nih.gov/tools/primer-blast/) with exon-exon junction span and specificity check for appropriate species (Chow et al., 2016). Primers were checked against mouse liver and human hepatocellular carcinoma cell (HepG2) or human liver tissue mRNA and water for specificity, and the sequences are summarized in Supplemental Table 1. mRNA was synthesized into cDNA by a High Capacity cDNA synthesis kit (Applied Biosystems by Life Technologies, Burlington, ON); cDNA was quantified by the Applied Biosystems 7500 series system using SYBR Green or TaqMan for detection. For human liver mRNA analysis, genes were normalized to human glyceraldehyde-3-phosphate dehydrogenase (GAPDH) (detects human). For mouse liver mRNA analysis, genes for mouse hepatocytes and nonparenchymal cells were normalized to mouse β-actin (detects mouse), and genes for cholangiocytes were normalized to mouse CK19 (detects mouse), a marker for cholangiocytes. Target gene data in mouse tissue was normalized to cyclophilin for brain and kidney, and to villin for the small intestine.

Western Blotting. Protein isolation was performed as previously described (Chow et al., 2009). Liver homogenate protein samples (25 μg) were loaded and separated by 12% SDS-polyacrylamide gels, transferred onto nitrocellulose membranes (Amersham Biosciences, Piscataway, NJ), then blocked with 5% (w/v) skim milk in Tris-buffered saline and 0.1% Tween 20 (TBS-T; SigmaAldrich Canada) for 1 hour at room temperature, followed by washes with 0.1% TBS-T. Primary antibody solutions of total ERK (1:5000 dilution) (cat. no. 9102; Cell Signaling Technologies, Danvers, MA) and pERK (1:1000 dilution) (cat. no. 9101; Cell Signaling Technologies) or GAPDH/Gapdh (1:10000 dilution) (cat. no. ab8245; Abcam, Cambridge, MA) were prepared in 5% skim milk in 0.1% TBS-T and incubated overnight at 4°C. On the next day, the membrane was washed with 0.1% TBS-T and then incubated with secondary antibody (1:2000 anti-rabbit or 1:10000 anti-mouse) in 2% skim milk in 0.1% TBS-T for 2 hours at room temperature, and then washed with 0.1% TBS-T. Bands were visualized with chemiluminescence reagents (Amersham Biosciences) and quantified by scanning densitometry. Two bands appeared for pERK and total ERK. The intensity for each of the 44- and 42-kDa bands was normalized individually to GAPDH/Gapdh (37 kDa) and summed for pERK or total ERK. The ratio of pERK/total ERK was then calculated.

Statistics. Data were expressed as mean ± S.E.M. for all data. For comparison between two groups, the two-tailed paired Student's *t* test was used. The value of $P < 0.05$ was set as the level of significance.

Results

Characteristics of FRGN, mFRGN, and hFRGN Mice

Liver weights of hFRGN mice were significantly greater than those of FRGN mice, although the liver and brain weights of mFRGN mice were smaller than those of FRGN mice (Table 4). The gross appearance of hFRGN livers appeared necrotic and consisted of multiple smaller lobes with distended gallbladders compared with of FRGN livers (Fig. 1A). mFRGN livers appeared abnormal and different, but less frequently so. All three mouse species showed higher than baseline plasma ALT levels owing to the withdrawal of NTBC (the supplement that rescues the liver from toxicity owing to absence of *Fah* gene) 3 days prior to experimentation. For the FRGN mouse, NTBC withdrawal resulted in some degree of liver damage, shown by the slightly elevated ALT levels. For the mFRGN mice, the ALT level was close to baseline values (~20 IU/ml), suggesting that the foreign mouse hepatocytes were able to replace damaged naïve mouse hepatocytes and restore liver function and lessen toxicity. For the hFRGN mice, the ALT level was the highest, relative to those in FRGN and mFRGN mice. The reason may be the presence of excessive bile acids (discussed later) found in the hFRGN system. Moreover, hFRGN mice contained much higher levels of liver cholesterol and conjugated bilirubin than those for FRGN mice (Table 4). Hepatic triglyceride levels in mFRGN livers (7.36 ± 1.57 mg/g) were higher than those of FRGN and hFRGN livers, although levels in hFRGN livers (3.3 ± 1.06 mg/g) were not significantly different from that in FRGN livers (1.81 ± 0.62 mg/g; Table 4). These observations were consistent with histopathological images with lipid Oil Red O staining (Fig. 1B).

Bile Acid Composition in Bile, Plasma, and Liver and Bile Acid Pool Sizes in FRGN, mFRGN, and hFRGN Mice

The composition of bile acids among FRGN, mFRGN, and hFRGN mice was compared (Fig. 2A; Table 5). In FRGN and

TABLE 4
Physiologic parameters of FRGN, mFRGN, and hFRGN mice (n = 4–9)

	FRGN	mFRGN	hFRGN
Body weight (g)	32.1 ± 3.6	33.0 ± 7.6	30.6 ± 4.0
Liver (% body weight)	7.61 ± 0.27	4.95 ± 0.14†	10.6 ± 0.31*
Brain (% body weight)	1.55 ± 0.07	1.27 ± 0.06†	1.56 ± 0.11
Kidney (% body weight)	2.08 ± 0.18	1.82 ± 0.14	2.24 ± 0.16
Plasma ALT (IU/ml)	113 ± 15.5	52.2 ± 17.0†	215 ± 30.1*
Plasma cholesterol (mg/dl)	151 ± 11.8	161 ± 11.0	152 ± 15.6
Liver cholesterol (mg/g)	2.17 ± 0.22	2.63 ± 0.20	3.14 ± 0.21*
Liver triglyceride (mg/g)	1.81 ± 0.62	7.36 ± 1.57†	3.31 ± 1.05
Total biliary bilirubin in bile (mg/dl)	5.0 ± 0.8	NM	11.6 ± 4.7
Conjugated bilirubin in bile (mg/dl)	1.0 ± 0.2	NM	4.9 ± 1.8*

NM, not measured.
†Denotes $P < 0.05$ compared between mFRGN and FRGN mice using two-tailed Student's t test.
*Denotes $P < 0.05$ compared between hFRGN and FRGN mice using two-tailed Student's t test.

mFRGN mice, muricholic acids (α-MCA, β-MCA, and ω-MCA) and their tauro-conjugates, as well as tCA were the major murine bile acids present in all biologic matrices (Fig. 2A; Table 5). Overall, implantation of foreign mouse hepatocytes into FRGN recipients did not greatly alter the bile acid composition in all biologic matrices (Fig. 2A), although bile acid concentrations in mFRGN mice were about 1.5- to 3.3-fold higher than those in FRGN mice (Table 5). For hFRGN mice, dramatic changes in bile acid composition and dramatically higher (by several to a few thousand-fold) bile acid levels over those of FRGN mice were observed in bile, plasma, and liver (Fig. 2A, Table 5). There were considerably greater glycine-conjugates, as expected of human bile acids, although taurine conjugates were also observed. Muricholic acid and variants of murine designation persisted in hFRGN plasma, bile, and liver. These differences in bile acid composition may have been contributed by many external factors. For the comparison in humans, it must be kept in mind that the human hepatocytes repopulated in these hFRGN livers were from either male or female donors, and gender difference in bile acid metabolism can occur (Fisher and Yousef, 1973); humanization of these livers originating from both male and female donors were indeed highly variable (Chow et al., 2016). In addition, gut microbiota are different between mice and humans, and this may contribute further to differences in secondary bile acid production (Wahlstrom et al., 2016).

Bile. In hFRGN bile, CA, CDCA, and DCA and their taurine- and glycine-conjugates, major forms found in humans, were observed to be significantly higher compared with those in FRGN bile (Table 5); DCA, gDCA, tDCA, tUDCA, gUDCA, tLCA, gLCA, α-MCA, and tα-MCA were also considerably higher in hFRGN bile. A detailed comparison of the bile

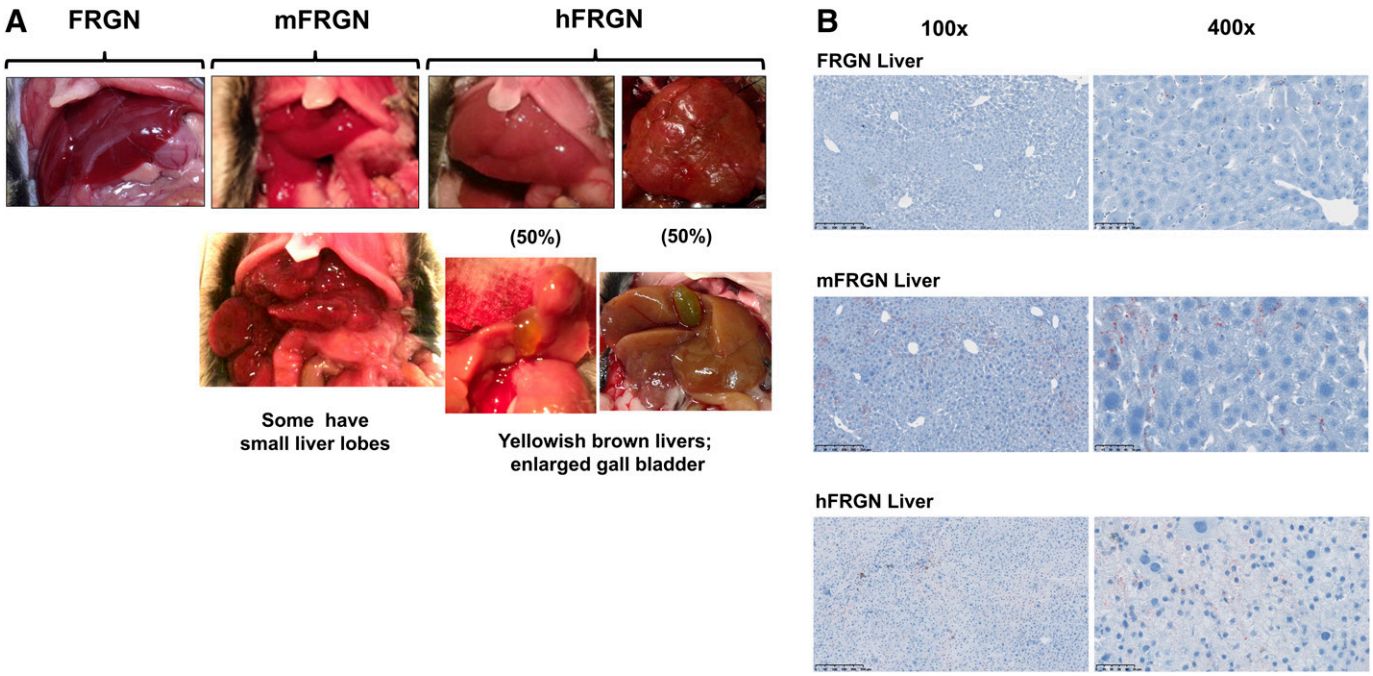

Fig. 1. Appearance of the FRGN, mFRGN, and hFRGN livers. (A) Gross appearance. Note the abnormal gross appearance, the distended gallbladder, small lobes, and the necrotic tissue in hFRGN livers. (B) Oil Red O staining at 100× (scaling from 0–250 μm with interval of 50 μm) and 400× magnifications (scaling from 0–50 μm with interval of 10 μm) of FRGN, mFRGN, and hFRGN livers (one representative preparation each). Normal morphology was observed in FRGN livers, whereas mFRGN livers showed higher lipid deposits than FRGN livers, whereas lipid deposits in hFRGN livers were only slightly higher. Hepatocytes appeared tightly packed in hFRGN livers.

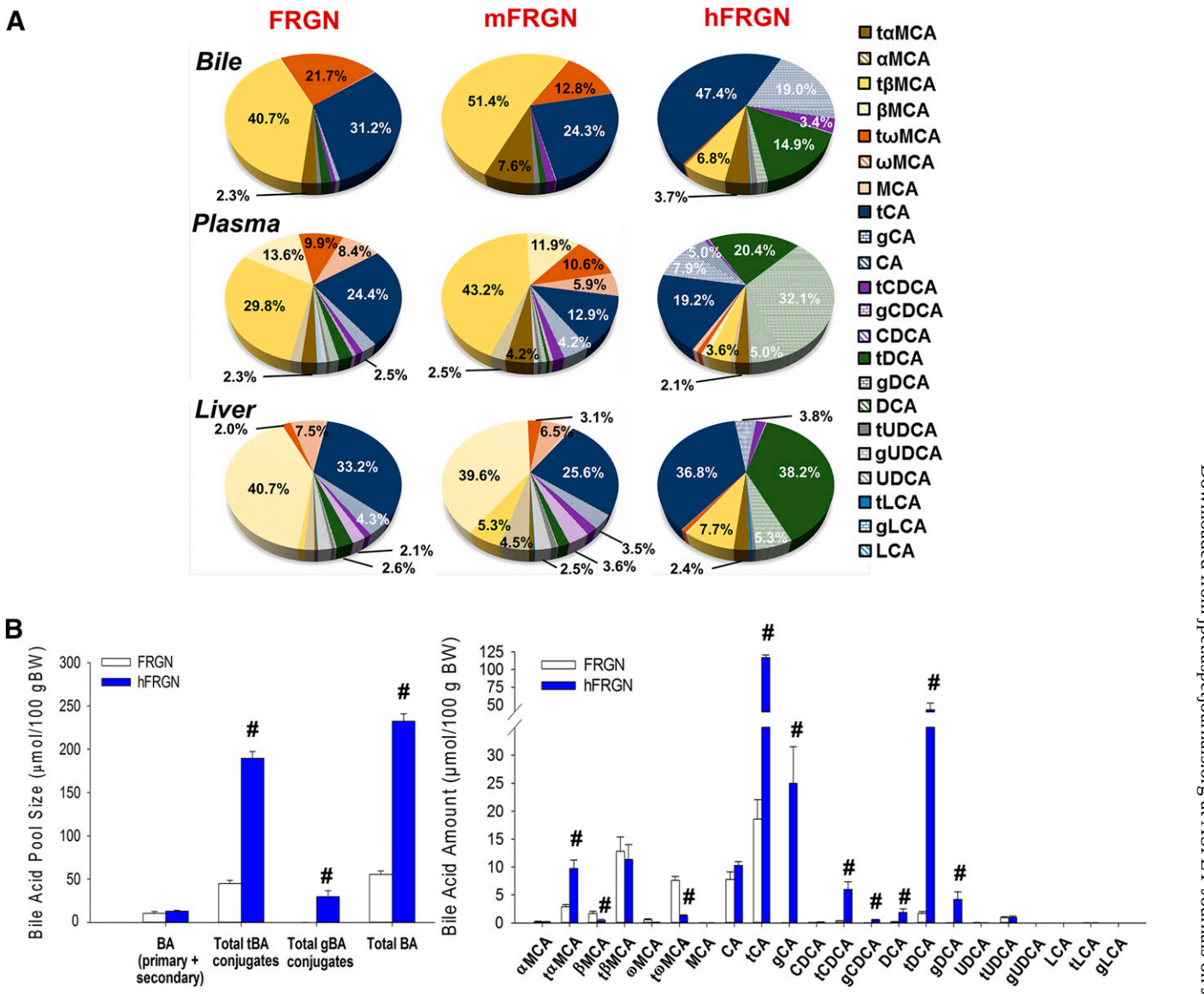

Fig. 2. Bile acid composition in (A) bile, plasma, and liver and (B) bile acid pool size (n = 4–8). Note that for hFRGN mice, there were much higher proportions of CDCA, CA, and DCA and their taurine-conjugates (>85% composition), which are strong FXR ligands, whereas for FRGN and mFRGN mice, these were 17–44%. By contrast, murine bile acids, muricholic acid (MCA), α-MCA, β-MCA, and ω-MCA and their taurine-conjugates, were 53–81% in FRGN and mFRGN mice and were 13–15% for hFRGN mice. The bile acid pool size was 4.2-fold higher for hFRGN than for FRGN mice. Data are mean ± S.E.M.; $^{\#}P < .05$, between FRGN and hFRGN mice, using a two-tailed Student's t test.

contents for hFRGN (including FRGN and mFRGN bile) and human bile was further conducted (Table 6). Even though levels of the glycine-conjugates of CA, DCA, CDCA, and UDCA were present in hFRGN bile, suggesting human metabolic activities, these concentrations were lower relative to those in human bile (Table 6). Moreover, higher proportions of taurine-conjugates as well as muricholic acids (10% total), rodent-specific bile acids formed from Cyp2c70 (Takahashi et al., 2016), were observed in hFRGN bile, although these are normally absent in human bile. Species differences in the bile acid conjugation pathways between human and rodents raised serious questions about the contribution of murine hepatic activities in these highly humanized livers, inasmuch as bile acids are mostly glycinated in human livers but are taurine-conjugated in rodent livers (Sayin et al., 2013). The higher taurine- to glycine-conjugates in hFRGN mice suggests the presence of remnant mouse hepatocyte activities. In addition, β-MCA and CA, which are normally conjugated with taurine in rodents (Sayin et al., 2013), were present abundantly as 58% of biliary bile acids in hFRGN mice, contrasting with the 6.5% CA and 0% MCA observed for human bile (Table 6). These facts again suggest the persistence of murine hepatic activities.

Plasma. In plasma, higher levels of human bile acids were observed in hFRGN mice than in FRGN mice, and MCA and tMCAs (murine bile acids) in hFRGN plasma were also higher than those in FRGN plasma (Table 5). DCA, the highly toxic bile acid, and its conjugated forms, tDCA and gDCA, for hFRGN were > 220-fold those of FRGN (Table 5).

Liver. In liver, primary and secondary bile acids, such as MCAs and CDCA were significantly lower in hFRGN mice compared with those in FRGN mice, but DCA and taurine- and

TABLE 5
Bile acid concentrations in bile, plasma, and liver (data of Fig. 2A) of FRGN, mFRGN, and hFRGN livers (n = 4–8, mean ± S.E.M.)

	Bile (μM)				Plasma (μM)				Liver (nmol/g)			
	FRGN	mFRGN	hFRGN	hFRGN to FRGN Ratio	FRGN	mFRGN	hFRGN	hFRGN to FRGN Ratio	FRGN	mFRGN	hFRGN	hFRGN to FRGN Ratio
Total BA	23,137 ± 4290	77,369 ± 31,272	241,840 ± 47,453*	10.5	6.6 ± 3.1	13.3 ± 4.7	321 ± 40.1*	49	76.4 ± 24.2	121 ± 38.0	429 ± 42.2*	5.6
Primary + secondary BA	252 ± 98	288 ± 88	2752 ± 698*	10.9	2.4 ± 1.5	4.4 ± 2.5	39.4 ± 14.8*	17	44.8 ± 15.2	75.9 ± 25.6	8.1 ± 4.0*	0.2
Tauro-conjugated BA	22,857 ± 4262	77,027 ± 31,201	183,520 ± 32,047*	8	4.2 ± 1.6	8.9 ± 3.1	153 ± 29.1*	37	31.3 ± 10.2	45.5 ± 12.6	382 ± 39.8*	12
Glyco-conjugated BA	28 ± 10	52 ± 33	55,567 ± 17,757*	2,003	<0.01	<0.01	129 ± 36.6*	∞[a]	0.16 ± 0.09	<0.01	39.3 ± 9.7*	240
α-MCA	9.3 ± 4.8	24.9 ± 11.3	88.0 ± 17.3*	9.5	0.09 ± 0.05	0.56 ± 0.34	1.81 ± 0.97	20.1	1.08 ± 0.32	4.61 ± 0.97	0.35 ± 0.12*	0.32
tα-MCA	522 ± 150	5580 ± 1,904	9536 ± 3,077*	18.3	0.13 ± 0.04	0.55 ± 0.21	7.13 ± 2.93*	55	0.32 ± 0.18	0.91 ± 0.30	9.17 ± 2.12*	29
β-MCA	63.3 ± 22.9	143 ± 41.8	95.6 ± 19.2	1.5	1.22 ± 0.91	1.83 ± 1.21	3.11 ± 0.60	2.5	31.7 ± 11.8	54.6 ± 21.9	1.23 ± 0.24*	0.04
tβ-MCA	9507 ± 2720	35,606 ± 11,721	16,354 ± 3,530	1.7	1.93 ± 0.89	5.26 ± 1.98	11.8 ± 2.67*	6.1	0.75 ± 0.38	8.14 ± 4.54	31.2 ± 3.52*	42
ω-MCA	61.6 ± 27.6	68.7 ± 21.9	24.5 ± 5.3	0.4	0.64 ± 0.39	0.98 ± 0.75	2.43 ± 0.65	3.8	5.84 ± 2.3	7.51 ± 2.88	0.35 ± 0.08*	0.06
tω-MCA	4863 ± 1,265	11,766 ± 5,849	1021 ± 308*	0.21	0.58 ± 0.22	1.31 ± 0.47	2.61 ± 0.48*	4.5	1.71 ± 0.99	4.03 ± 1.67	3.23 ± 0.92	1.9
MCA	0.1 ± 0.15	<0.01	1.4 ± 0.68	14	0.01 ± 0	0.01 ± 0.01	0.10 ± 0.02*	10	0.49 ± 0.17	0.63 ± 0.13	0.03 ± 0.01*	0.06
CA	117 ± 47	51 ± 16	2502 ± 680*	21.3	0.2 ± 0.1	0.7 ± 0.6	16.2 ± 12.3*	76	2.89 ± 1.05	3.22 ± 0.68	4.58 ± 3.36	1.6
tCA	7318 ± 1484	22,085 ± 11,681	109,010 ± 24,806*	14.9	1.33 ± 0.49	1.47 ± 0.50	61.4 ± 16.9*	46	25.1 ± 8.4	28.1 ± 7.5	165 ± 36.4*	6.6
gCA	28 ± 10	52 ± 32	50,400 ± 15,742*	1,816	<0.01	<0.01	24.4 ± 10.9*	∞	0.08 ± 0.05	<0.01	17.1 ± 7.0*	207
CDCA	<0.01	<0.01	1.96 ± 0.27*	∞	0.04 ± 0.02	0.09 ± 0.06	0.37 ± 0.04*	9.2	1.35 ± 0.36	3.06 ± 0.46	<0.01*	<0.01
tCDCA	160 ± 33	763 ± 123†	8,503 ± 3,440*	53	0.07 ± 0.03	0.20 ± 0.07	2.61 ± 0.98*	38	0.80 ± 0.23	1.77 ± 0.41	8.47 ± 1.84*	10
gCDCA	<0.01	<0.01	671 ± 287*	∞	<0.01	<0.01	0.43 ± 0.15*	∞	<0.01	<0.01	0.87 ± 0.27*	∞
DCA	<0.01	<0.01	38.5 ± 12.2*	∞	0.07 ± 0.01	0.12 ± 0.03	14.8 ± 2.41*	221	0.16 ± 0.07	0.14 ± 0.02	1.54 ± 0.67*	9.8
tDCA	367 ± 262	581 ± 151	36,171 ± 12,732*	99	0.09 ± 0.03	0.06 ± 0.02	66.8 ± 14.7*	725	2.23 ± 1.16	1.46 ± 0.21	161 ± 18.8*	72
gDCA	<0.01	<0.01	4200 ± 1925*	∞	<0.01	<0.01	103 ± 29.6*	∞	0.06 ± 0.03	<0.01	21.2 ± 4.9*	348
UDCA	0.8 ± 0.2	1.1 ± 0.3	0.5 ± 0.3	0.63	0.06 ± 0.04	0.09 ± 0.03	0.13 ± 0.02	2.2	1.33 ± 0.28	2.12 ± 0.58	<0.01*	<0.01
tUDCA	116 ± 28	630 ± 237†	2654 ± 1396*	22.9	0.03 ± 0.01	0.07 ± 0.02	0.38 ± 0.11*	12.7	0.38 ± 0.18	0.88 ± 0.20	1.74 ± 0.25*	4.6
gUDCA	<0.01	<0.01	277 ± 157*	∞	<0.01	<0.01	<0.01	NA	<0.01	<0.01	0.08 ± 0.08	NA
LCA	<0.01	<0.01	<0.01	NA	0.05 ± 0.03	<0.01	0.02 ± 0.01	0.4	<0.01	<0.01	<0.01	NA
tLCA	2.7 ± 1.2	14.4 ± 3.7†	269 ± 131*	100	<0.01	<0.01	0.14 ± 0.07	∞	0.08 ± 0.01	0.18 ± 0.06	1.74 ± 0.43*	22
gLCA	<0.01	<0.01	17.9 ± 8.1*	∞	<0.01	<0.01	0.31 ± 0.11*	∞	0.02 ± 0.02	<0.01	0.07 ± 0.02	3.5

†and * denote $P < 0.05$ compared between mFRGN and FRGN mice and hFRGN and FRGN mice, respectively, using two-tailed Student's t test or Mann-Whitney test; NA, not applicable.
[a] ∞

TABLE 6
Comparison of biliary bile acid composition to that in healthy adults according to Rossi et al. (1987) in human bile (t and g denote taurine- and glycine-conjugated bile acids, respectively)

	(% Assayed Bile Species)			
	FRGN	mFRGN	hFRGN	Humans
CA	0.52	0.09	1.41	
tCA	31.2	24.3	47.4	6.5
gCA	0.11	0.05	19.0	34.1
DCA	0	0	0.02	
tDCA	1.50	0.98	14.9	2.1
gDCA	0	0	1.59	13.6
CDCA	0	0	0	
tCDCA	0.69	1.40	3.44	5.1
gCDCA	0	0	0.25	28.9
UDCA	0	0	0	
tUDCA	0.64	0.88	0.89	0.9
gUDCA	0	0	0.09	1.5
α-MCA	0.04	0.04	0.04	0
tα-MCA	2.29	7.61	3.74	0
β-MCA	0.28	0.23	0.05	0
tβ-MCA	40.7	51.4	6.76	0
ω-MCA	0.27	0.11	0.01	0
tω-MCA	21.7	12.8	0.40	0
tLCA	0.01	0.03	0.12	0.1
tLCA-sulfate	Not assayed	Not assayed	Not assayed	0.2
gLCA	0	0	0.01	0.6
gLCA-sulfate	Not assayed	Not assayed	Not assayed	0.2
Unknown others	Not assayed	Not assayed	Not assayed	6.0

glycine-conjugated bile acids were 9.8x, 72x and 348x higher, respectively (Table 5). The murine bile acids were higher in hFRGN livers: tα-MCA, tβ-MCA, and tω-MCA concentrations in hFRGN livers were 29-, 42-, and 1.9-fold those in FRGN liver, respectively (Table 5).

Bile Acid Pool Sizes. The extremely high levels of bile acids in bile, plasma, and liver observed in hFRGN mice prompted us to compare the bile acid pool sizes between hFRGN and FRGN mice. The bile acid pool size for hFRGN mice ($n = 4$) was found to be 4.2-fold that of FRGN mice ($n = 4$) (Fig. 2B). Human conjugated bile acids such as tCDCA, tDCA, tUDCA, tLCA, gCA, gCDCA, gDCA, gDCA were significantly higher in hFRGN mice, and the MCA content in hFRGN mice was proportionately lower, although not absent. Glycoconjugates, tauro-conjugates, and DCA were almost 1,000-fold (gCDCA, 2,220-fold; gCA, 943-fold; gDCA, 1,140-fold), 4.2-fold (tDCA, 26-fold; tCA, 6.3-fold), and 8.7-fold higher in hFRGN mice, respectively (Fig. 2B). The presence of the much higher proportions of DCA, tDCA and gDCA, highly toxic bile acids, would render greater toxicity to the liver (Delzenne et al., 1992).

Comparison of Basal Human mRNA Expression between hFRGN Livers and Normal Human Liver Tissues

hFRGN livers and human liver tissues were examined to compare basal human mRNA and other underlying changes. For examination of whether any of the bile acid synthetic pathways were altered, mouse and human enzymes in hFRGN livers and human liver tissues were measured (Fig. 3). CYP7A1, or CYP 7α-hydroxylase, the rate-limiting enzyme for the classic (major) pathway in bile acid synthesis; oxysterol 7α-hydroxylase or CYP7B1, the rate limiting enzyme in the alternative (acidic) pathway for CDCA production; CYP27A1, the alternative enzyme for CDCA production in both the classic and alternative pathways; and murine/human bile acid CoA/amino acid *N*-acyltransferase (BAAT; conjugative enzyme) (Chiang, 2009) were evaluated. As shown in Fig. 3A, there was no difference in human hepatic CYP27A1, CYP7B1, and BAAT mRNA expression between hFRGN livers and human livers, except for human CYP7A1 mRNA expression, which was 120-fold higher in hFRGN over human liver tissue (Fig. 3A). By contrast, mouse liver Cyp7b1, Cyp27a1, and Baat mRNA expression (Fig. 3B) in hFRGN livers were much lower than those for FRGN and mFRGN mice.

The mRNA expression of human CAR, human hepatocyte nuclear factor 4 alpha (HNF-4α), peroxisome proliferator-activated receptor (PPARγ), albumin, β-Klotho, CYP2E1, glutathione *S*-transferase (GSTA4-4), UGT1A1, organic anion–transporting polypeptides (OATP1B1 and OATP1B3), bile salt export pump (BSEP), ABCG5, ABCG8, OSTα–OSTβ, multidrug resistance protein 1 (MDR1), and multidrug resistance–associated protein 2 (MRP2) were also higher (1.5- to 2.5-fold) in hFRGN livers over those in human liver tissue (Fig. 3A), whereas those for FXR and SHP were lower in hFRGN livers. One plausible reason for the lower FXR expression is the presence of extremely high levels of taurine-conjugated MCAs (Table 5), FXR antagonists (Sayin et al., 2013); inhibition of FXR would lead to the reduction in SHP expression (Fig. 3A). Those for CYP1A1, CYP2C19, breast cancer resistance protein (BCRP), OSTα, and OSTβ mRNA levels in hFRGN livers were 2.5-fold higher, with a notable 100-fold higher CYP7A1 mRNA level in hFRGN livers compared with those in human liver tissue (Fig. 3A). Despite the high bile acid contents in hFRGN livers (Table 5), the mRNA expression of MRP3, a bile acid–associated FXR target, was unexpectedly lower (Fig. 3A).

Miscommunication among Human Hepatocytes and Murine Nonparenchymal Cells (Mouse Kupffer Cells, Stellate Cells, and Cholangiocytes) in hFRGN versus FRGN and mFRGN Livers

The communication between human hepatocytes and mouse nonparenchymal cells in hFRGN livers was evaluated

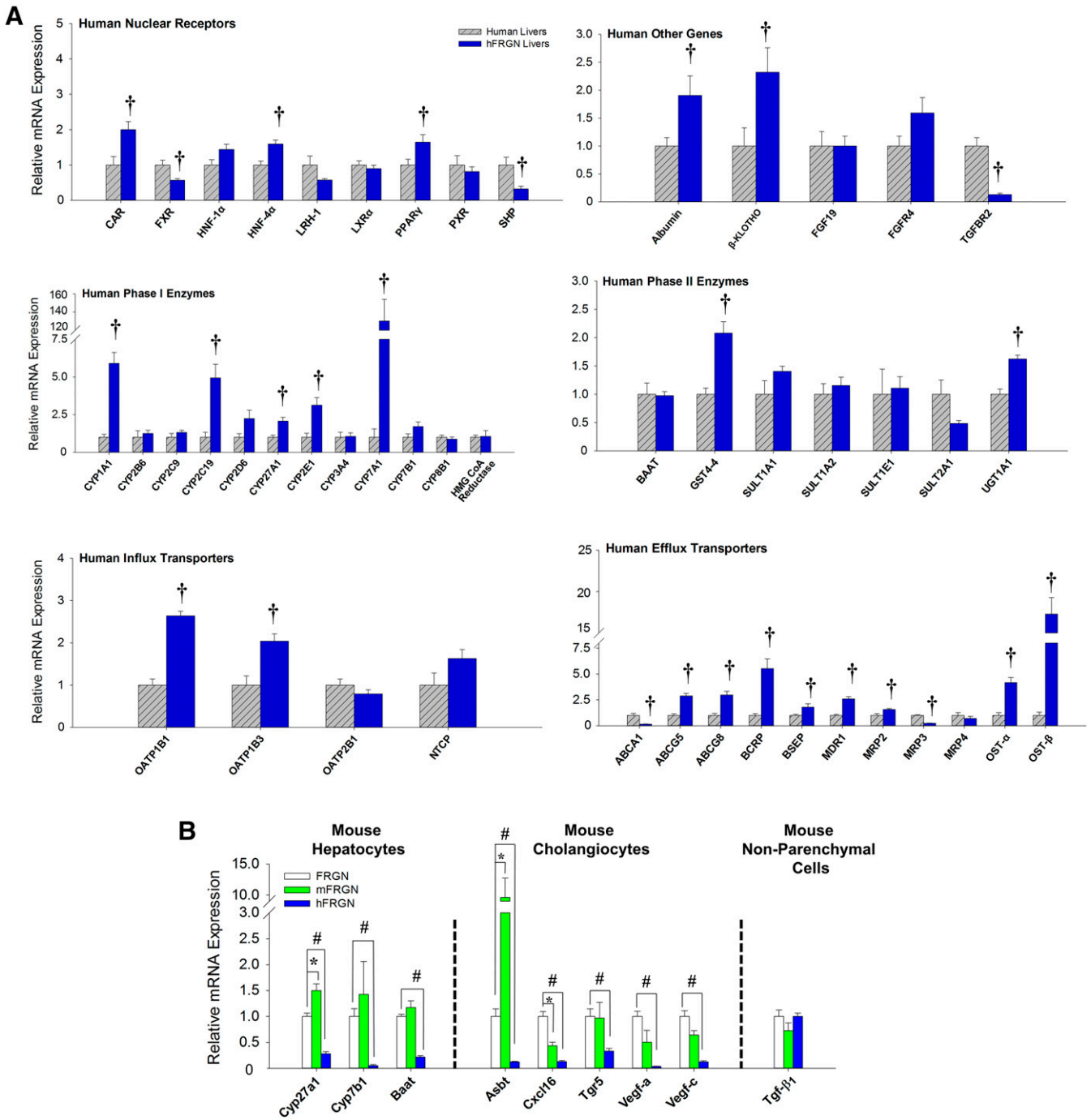

Fig. 3. Hepatic mRNA expression of (A) human genes in hFRGN livers ($n = 11$) and those in human liver tissues ($n = 6$) and (B) murine genes present in FRGN, mFRGN, and hFRGN livers ($n = 4$–8). Hepatic human mRNA expression in hFRGN livers was generally higher than in human liver tissue, whereas FXR and SHP mRNA expression was significantly lower (A). Mouse Tgf-β1, the antiproliferative gene in nonparenchymal cells, was unchanged, whereas mRNA expression of other murine bile acid metabolic enzymes in mouse hepatocytes and murine proliferative markers and apical sodium-dependent bile acid transporter (Asbt) in cholangiocytes were lower in hFRGN livers (B). Data are mean ± S.E.M.; $^{\dagger}P < .05$, between human livers and hFRGN livers; $^{*}P < .05$, between FRGN and mFRGN livers; $^{\#}P < .05$, between FRGN and hFRGN livers, using a two-tailed Student's t test.

to assess the proliferation status. Since the transforming growth factor beta receptor 2 (TGFBR2) in human hepatocytes, and Tgf-β1 that is produced by a multitude of mouse nonparenchymal cells, including Kupffer cells, sinusoidal endothelial cells, dendritic cells and stellate cells (De Bleser et al., 1997; Schon and Weiskirchen, 2014; Weiskirchen and Tacke, 2014) are both antimitogenic, these termination signals were evaluated. TGFBR2 mRNA expression in hFRGN livers was significantly lower, only 10% that in normal human liver tissue (Fig. 3A), suggesting continuous hepatocyte proliferation in hFRGN livers. In addition, mouse Tgf-β1 mRNA level in hFRGN was not elevated compared with that in FRGN livers (Fig. 3B), suggesting that mouse stellate/Kupffer cells failed to respond to the high number of human hepatocytes present in hFRGN livers (Yoshizato et al., 2012). These results suggest a lack of communication

between mouse stellate cells and human hepatocytes that can lead to continuous proliferation.

To examine further whether proliferation of hepatocytes had influenced cholangiocyte growth and intrahepatic bile acid mass, chemokine (C-X-C motif) ligand 16 (Cxcl16) (Omenetti et al., 2009) and other vascular endothelial growth factors (Vegf-a and Vegf-c) (Glaser et al., 2014; Meng et al., 2014), key cell-growth proliferators in cholangiocytes, were measured (Fig. 3B). The results showed that these markers were significantly decreased, suggesting that murine cholangiocyte proliferation was inhibited. In addition, expression of the transmembrane-bound G protein-coupled receptor (Tgr5) that is activated by bile acids (especially tLCA and tDCA) (Keitel and Haussinger, 2013; Duboc et al., 2014; Reich et al., 2016) and localized in cholangiocytes and modulates cholangiocyte proliferation and bile flow, was lower (Fig. 3B). The apical sodium-dependent bile acid transporter (Asbt), regulated by cAMP and Tgr5 (Xia et al., 2006; Keitel and Haussinger, 2013) in cholangiocytes, was also lower in hFRGN livers (Fig. 3B). The results suggest a decrease in cholangiocyte proliferation and bile acid reuptake (Lazaridis et al., 1997). The expected consequence of downregulated Tgr5 in hFRGN livers is a reduction of the cholehepatic shunt, leading to higher bile acid concentration in bile and the possibility of generating cystic fibrosis or primary sclerosing cholangitis characteristics (Glaser and Alpini, 2009; Maroni et al., 2015).

Proteomics of Human/Murine Liver Protein Abundances in hFRGN Livers

To investigate the potential role of bile acid dysregulation in the hFRGN liver, we performed proteomic analysis, the more quantitative tool to differentiate between human and mouse proteins in hFRGN livers, to evaluate the absolute transporter and enzyme changes (Fig. 4). As with the mRNA data (Fig. 3A), the protein expression of human CYP7A1, determined by LC-MS/MS, was higher (>3-fold) in hFRGN livers than that in human liver tissue (Fig. 4A). The protein expression of mouse Cyp7a1, the rate-limiting enzyme in cholesterol metabolism, in hFRGN livers was only slightly lower compared with that in FRGN livers, suggesting that the contribution of murine enzyme for bile acid synthesis in hFRGN liver would not be negligible despite Cyp27a1 and Cyp7b1 mRNA expression

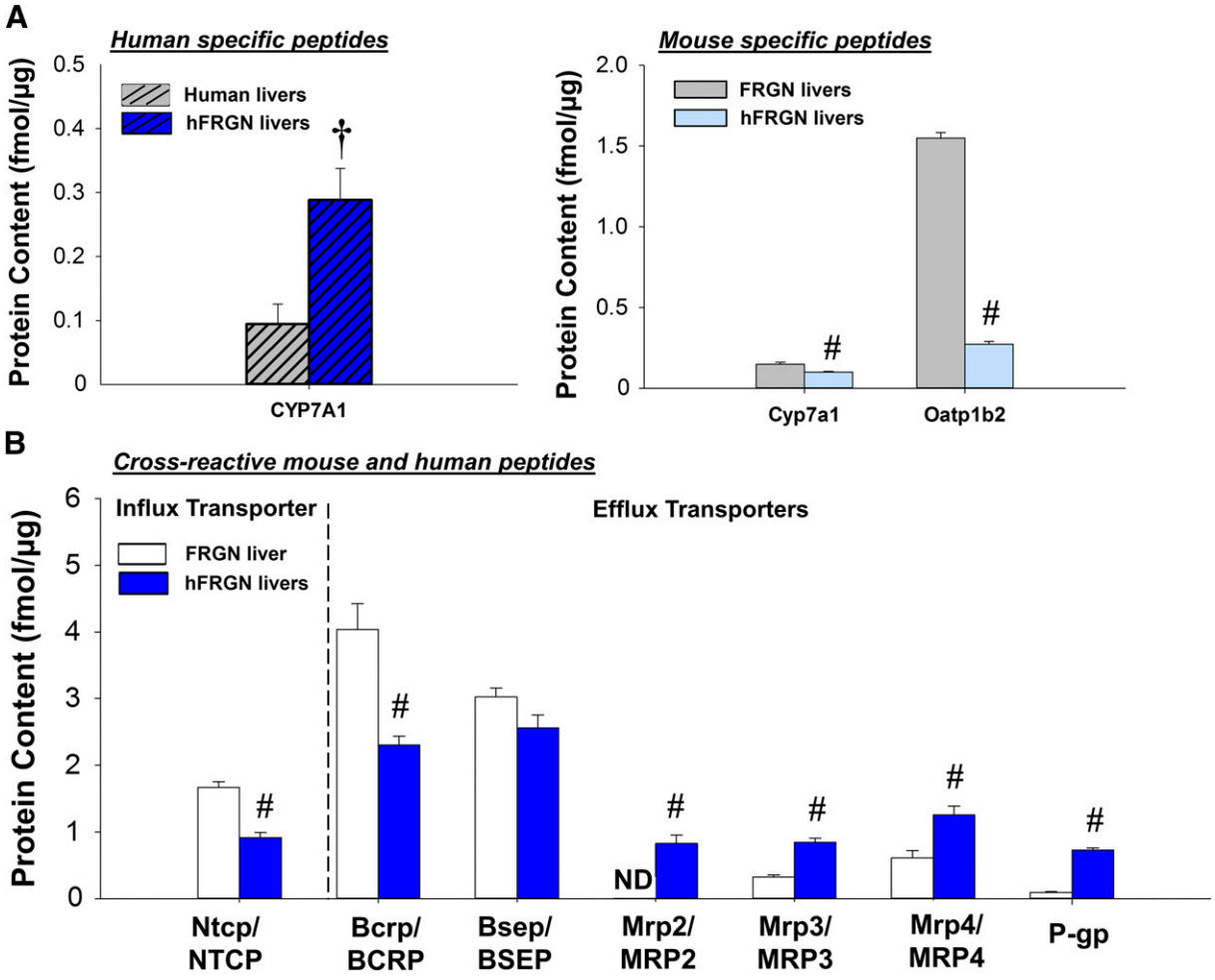

Fig. 4. Proteomics of liver proteins. (A) With the human-specific peptide, liver CYP7A1 protein level was found to be >3-fold higher in hFRGN livers (n = 9) than in human liver tissues (n = 3); with mouse-specific peptides, murine Cyp7a1 level was found to be comparable to that of FRGN livers, and murine Oatp1b2 protein persisted in hFRGN liver. (B) Cross-reactive (mouse + human) peptides were also used to detect liver proteins in hFRGN and FRGN livers (n = 6–8). Data are mean ± S.E.M.; ND denotes not detected/below detection limit; $^{\dagger}P < 0.05$, between hFRGN and human livers; $^{\#}P < .05$, between FRGN and hFRGN livers, using a two-tailed Student's t test.

levels being much lower (Fig. 4B). Remnant protein expression of murine Oatp1b2, the ortholog of human OATP1B1 and OATP1B3 (Evers and Chu, 2008), was also observed (Fig. 4B). Owing to a lack of species specificity in protein sequence [sodium-dependent taurocholate–cotransporting polypeptide (Ntcp/NTCP), Bcrp/BCRP, Bsep/BSEP, Mrp2/MRP2, Mrp3/MRP3, Mrp4/MRP4, and P-glycoprotein (P-gp)] of the peptides, a comparison between the amounts of human- and mouse-specific protein in hFRGN and FRGN livers could not be made in the proteomic analyses. Rather, the comparison was conducted using either mouse-specific or cross-reactive peptide for the target proteins in FRGN and hFRGN livers. In Fig. 4C, protein contents in Ntcp/NCTP and Bcrp/BCRP were found to be lower for hFRGN livers than for FRGN livers, whereas levels for the ATP transporters (Mrp2/MRP2, Mrp3/MRP3, and Mrp4/MRP4 and P-gp) were all higher. Protein differences of Ntcp/NTCP, Mrp4/MRP4, and murine/human P-gp in FRGN and hFRGN livers were consistent with those protein levels previously measured with immunoblotting (Chow et al., 2016), which may also be reflective of cross-reactive peptides. In addition, these protein data were consistent with those for mRNA expression that have been published (Chow et al., 2016).

Miscommunication between Human Hepatocytes and Murine Intestine

The potential Fgf15 and FGF19 signaling pathway on hepatic human CYP7A1 regulation in hFRGN mice was evaluated to assess the communication between murine intestine and human hepatocytes. Levels of FGF19 in liver, bile, gallbladder, and plasma, when assayed with ELISA, were found absent (data not shown). Levels of Fgf15 in plasma, though measured with ELISA, remained uncertain since the measured values are unreliable (personal communication with Dr. Steven A. Kliewer). Intestinal murine Fgf15 mRNA expression, therefore, served as a biomarker of what the circulating Fgf15 levels would have been. In hFRGN intestine, Fgf15 expression was significantly induced (500-fold), probably by intestinal Fxr activation (Fig. 5A), a line of reasoning that is supported by induction of all other intestinal Fxr targets, such as Ostα, mouse ileal bile acid binding protein (Ibabp), and Shp, since high levels of bile acid in hFRGN mice were observed (Fig. 2B). In addition, the apical sodium-dependent bile acid transporter (Asbt) expression (Fig. 5A) was lower in hFRGN intestine, probably owing to inhibition by the Fxr-Shp murine/human liver receptor homolog 1 (Lrh-1) cascade (Chen et al., 2003) or inhibition by Fgf15 (Sinha et al., 2008). Moreover, analyses of phosphorylated ERK (pERK) and total ERK protein (Fig. 5B), an indicator of FGFR4 activation in human hepatocytes, showed that both pERK and the ratio of pERK/total ERK were similar in FRGN and hFRGN livers, suggesting that the increase in Fgf15 did not result in higher activation of FGFR4/β-Klotho signaling pathway in human hepatocytes. As a result, CYP7A1 protein expression in hFRGN remained elevated compared with that for human liver tissue (Fig. 4A), drastically increasing the bile acid pool size in hFRGN mice (Fig. 2B).

Changes in Basal mRNA Expression in Other Mouse Tissue

Changes in nuclear receptor, transporter, and enzyme expression in the mouse intestine, kidney, and brain were also evaluated among FRGN, mFRGN, and hFRGN mice to assess the potential impact of bile acid dysregulation on interorgan communication.

Intestinal Genes. The basal mRNA levels of different intestinal genes were generally similar between FRGN and mFRGN intestine (Fig. 6). However, levels were much different between FRGN and hFRGN intestine. For important xenobiotic intestinal genes, higher Car and Pxr levels as well as Mdr1a, Mrp4, murine glutathione *S*-transferase (Gsta4-4), sulfotransferase (Sult1a1), and UDP-glucuronosyltransferases (Ugt1a1) were observed in hFRGN intestine (Fig. 6). Fluctuations in intestinal Oatp2b1 and Gsta3-3 were found in mFRGN and hFRGN intestine, and slightly lower intestinal Mrp3 (all three segments) and Bcrp (ileal segment) were observed for the hFRGN intestine. The basis for these differences is currently unknown since both higher LCA (a Pxr agonist) and human bile acids (strong Fxr agonist) coexisted in the intestine.

Renal Genes. Only minor differences in renal genes between mFRGN and FRGN mice were observed (Supplemental Fig. 1), and variations in Lxrα, Pxr, Oapt1a1, Oatp1a4, Ost-β, Oat1, Oat3 and Sult1a1 expression were small. However, when the basal expression of FRGN and hFRGN kidneys was compared, greater changes were observed. Renal Pxr and Car levels were found to be increased, and Lxrα levels were decreased in hFRGN mice. In addition, renal mRNA expression of Oatp1a4, Ost-α, Ost-β, Mrp2, Mrp3, Mrp4, and Gsta4-4 were all elevated in hFRGN mice, though vitamin D receptor (Vdr), Oapt1a1, Oat1, mouse oligopeptide transporter 2 (PepT2), and Cyp2e1 levels in hFRGN mice were lower compared with those of FRGN mice. The data suggest that many of the observed changes could have been the result of Fxr- and Pxr-mediated regulation resulting from the high levels of bile acids.

Brain Genes. Only minor changes in brain nuclear receptors and transporters were observed between mFRGN and FRGN mice (Supplemental Fig. 2). Changes in transporter were small, although expression of Oapt1a4, Oatp2b1, and Mdr1a levels were increased. Levels of Cyp1a2, Cyp2e1, Cyp3a11, Gsta3-3, and Ugt1a1 were significantly lower in hFRGN brain compared with those of FRGN brain.

Discussion

Development of the h-chimeric mouse liver model has been hailed as a useful in vivo tool for the study of human liver metabolism. Many studies supported the presence of human enzyme and transporter expression in humanized mouse livers (Katoh et al., 2005a, 2005c; Nishimura et al., 2005), and pharmacokinetic studies in humanized mice showed the presence of in vivo human metabolites (Okumura et al., 2007; Grompe and Strom, 2013; Bateman et al., 2014). However, other studies using chimeric models showed that the levels of in vivo human metabolites were unpredictable and different from those in humans (De Serres et al., 2011; Liu et al., 2011; Sanoh et al., 2012).

In our previous study, we identified two key issues on the discordance of the humanized model. We unveiled the presence of remnant native mouse hepatocytes and loss of metabolic zonation in hFRGN livers (Chow et al., 2016). In the present report, histopathologic, biologic, mRNA, and proteomics (using LC-MS/MS) data provided additional evidence to suggest

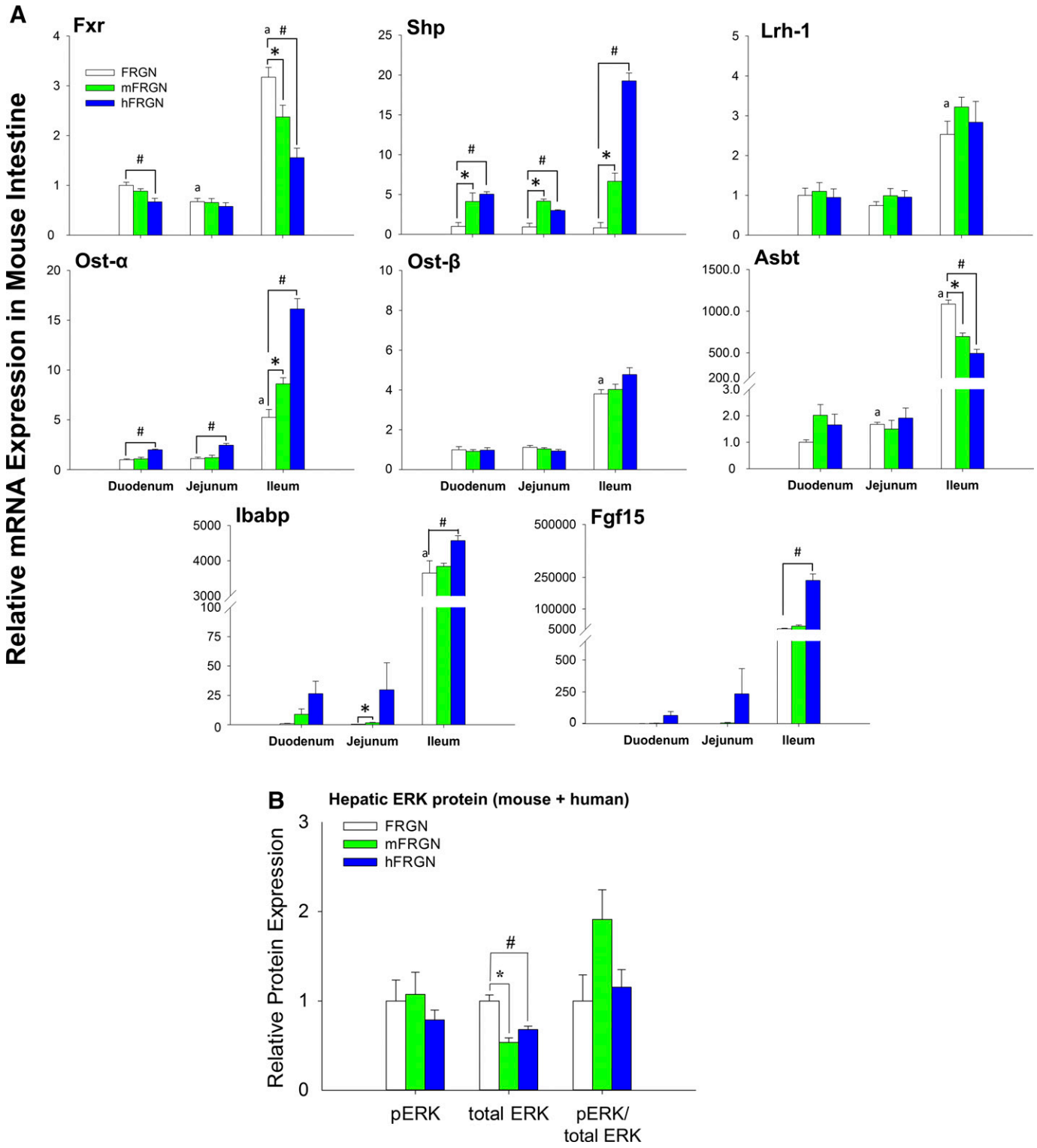

Fig. 5. (A) mRNA expression of murine intestinal nuclear receptors, enzymes, and transporters related to bile acid transport/metabolism and (B) the ratio of pERK/total ERK protein levels (in liver) as an activation indicator of the Fgf15-FGFR4 signaling pathway in FRGN, mFRGN, and hFRGN mice (n = 4–8). *$P < .05$, between FRGN and mFRGN intestine of same segment or liver; #$P < .05$, between FRGN and hFRGN intestine of same segment or liver; [a]$P < 0.05$, between FRGN duodenum and FRGN jejunum or ileum using two-tailed Student's t test.

instability of the model, including the 4.2-fold bile acid pool size, the much higher levels of the toxic bile acid, DCA, and its conjugates (Fig. 2B), the uncontrollable human hepatocyte proliferation and liver deformity (Figs. 1 and 3), bile acid dysregulation (Table 5; Fig. 2), toxicity (Table 4), enlarged gallbladder filling (Fig. 1A), and significant changes in extra-hepatic transporters and enzymes (Figs. 5 and 6, Supplemental Figs. 1 and 2). Although the model is being used increasingly as a tool for drug discovery and development to relate to human drug metabolism and toxicity, it is recognized that many of

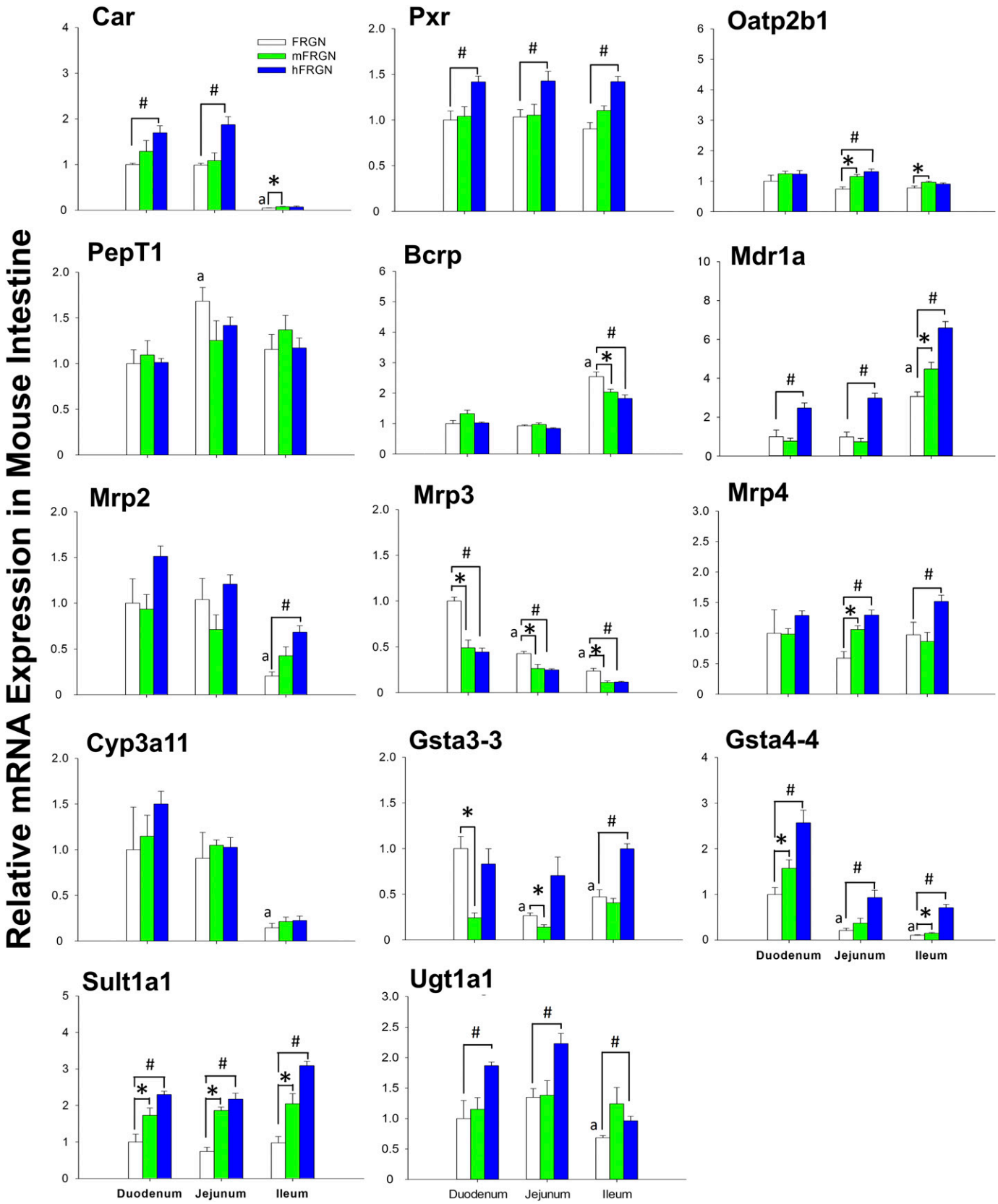

Fig. 6. In intestine, mRNA expression of mouse nuclear receptors, transporters, and enzymes in FRGN, mFRGN, and hFRGN mice (n = 4–8). Higher levels of Car and Pxr in hFRGN intestine were observed. Higher levels of Mdr1a, Mrp4, Gsta4-4, Sult1a1, and Ugt1a1 were present in most intestinal segments of hFRGN intestine, although higher Gsta4-4 and Sult1a1 expression, though lower Mrp3 and ileal Bcrp, was observed in mFRGN intestine (mechanism unknown); other changes between FRGN and mFRGN were minor. $^{*}P < 0.05$ denotes comparison between FRGN and mFRGN intestine of same segment; $^{\#}P < 0.05$ denotes comparison between FRGN and hFRGN intestine of same segment; $^{a}P < 0.05$, between FRGN duodenum and FRGN jejunum or ileum, using two-tailed Student's t test.

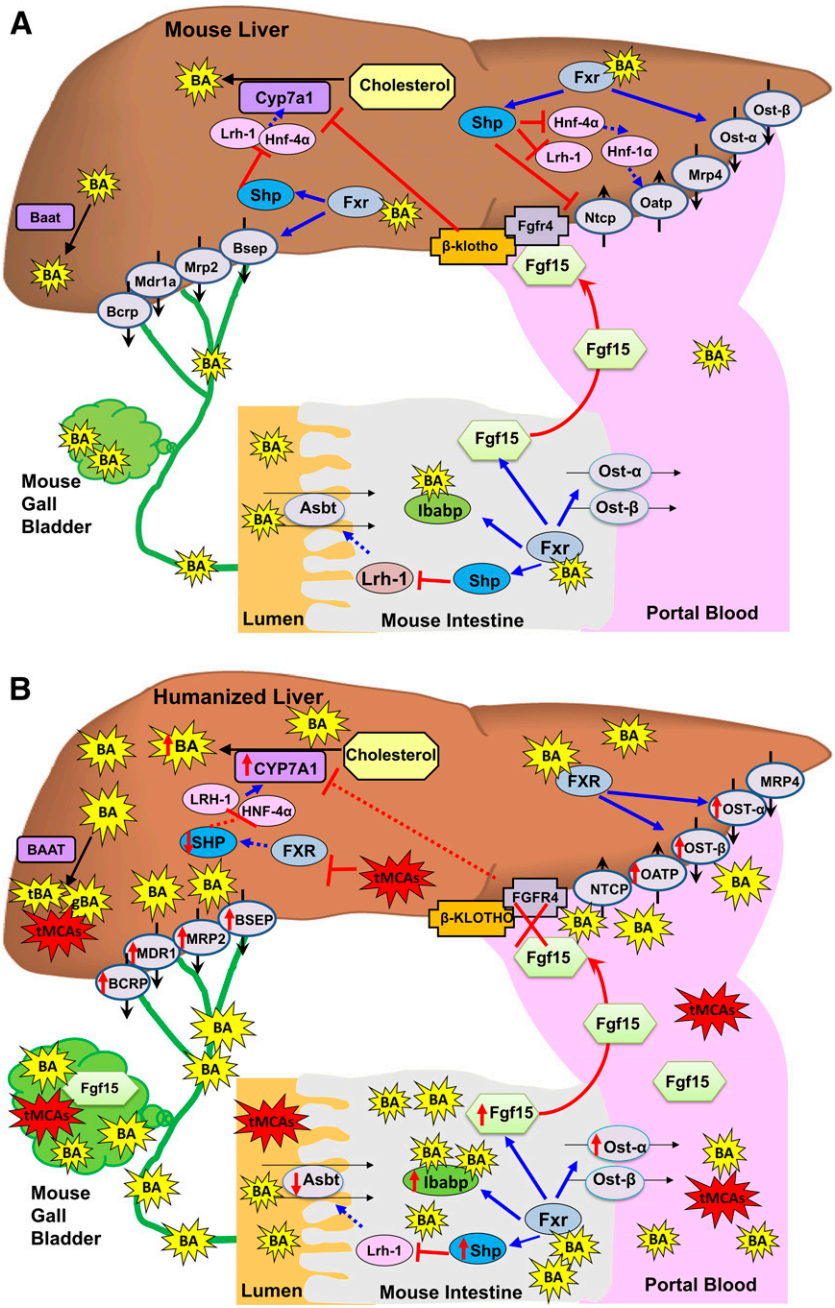

Fig. 7. Schematics depicting the interaction between (A) the murine intestine and murine liver and bile acids (denoted as BA), and (B) the murine intestine and humanized liver. (A) Normally, there are two major pathways for Cyp7a1 regulation: 1) in liver, by the Fxr-Shp-Lrh-1 or Hnf-4α cascade and 2) in murine intestine by Fgf15, secreted by the ileum and under Fxr stimulation, to react with Fgfr4 in liver to repress Cyp7a1. (B) Owing to the over-production of murine bile acids by the hFRGN liver, the conjugated MCAs that are strong FXR antagonists, inhibited liver FXR, whereas strong FXR ligands stimulated intestinal Fxr targets: murine Shp, Fgf15, Ibabp, and Ostα. However, miscommunication between the murine intestinal Fgf15 and human FGFR4 and inhibition of the liver FXR-SHP cascade failed to repress CYP7A1 expression. Consequently, CYP7A1 expression levels remained elevated for the synthesis of bile acids, and high BAs prevailed in this vicious circle. Note that blue lines represent stimulation, whereas red line represents inhibition. Solid line denotes activation/increased pathway, whereas dotted lines denote the absence/decrease of the pathway.

these deficiencies have been previously overlooked and not properly addressed.

Dysregulated liver regeneration and deformity in hFRGN livers were evidenced by the miscommunication between human hepatocytes and murine stellate cells, leading to substantial hepatocyte proliferation, reduced intracellular spaces (Chow et al., 2016), and inhibited cholangiocyte growth. The signaling in hepatocytes and nonparenchymal cells between TGFBR2/TGF-β plays a critical role in liver regeneration (Yoshizato et al., 2012). Studies with cultured hepatocytes have shown that TGF-β1 and TGFBR2 are antimitogenic for hepatocytes. Under normal resting (physiologic) condition, hepatocytes express TGFBR2, whereas nonparenchymal cells express low levels of TGF-β1. When the liver is injured, TGFBR2 expression in hepatocytes is reduced to initiate proliferation. Once an adequate number of hepatocytes is produced, the stellate cells surround the hepatocytes and produce TGF-β, which signals to hepatocytes to terminate proliferation and negatively inhibit TGF-β1 expression (Yoshizato et al., 2012). Our results showed that hFRGN livers consisted of remarkably lower TGFBR2 expression, but an unchanged murine Tgf-β1 expression compared to that for FRGN livers (Fig. 3). Histopathologic images from current (Fig. 1A) and previous studies (Chow et al., 2016) support the evidence of unchecked hepatocyte proliferation and densely populated liver (Fig. 1A). Invasive hepatocyte proliferation and inhibited cholangiocyte growth (Fig. 3B) resulted in reduced bile flow (Chow et al., 2016) and cholehepatic shunting and increased hepatic bile acid accumulation and toxicity (Tables 4 and 5). The densely populated hFRGN livers may further lead to ischemia within the acinus, a condition that leads to inhibition of FXR (Cheng et al., 2013).

The inability of humanized mouse livers to regulate CYP7A1 expression led to high bile acid levels and toxicity. Normally, Cyp7a1/CYP7A1 in liver is under Fxr/FXR and Fgf15/FGF19 control (Fig. 7A). At high bile acid levels, Fxr/FXR in the intestine activates intestinal Fgf15/FGF19, which forges an interaction with Fgfr4/FGFR4 to repress Cyp7a1/CYP7A1 (Inagaki et al., 2005). In liver, the FXR-SHP-LRH-1 or FXR-SHP-HNF-4α cascade negatively controls CYP7A1 (Goodwin and Kliewer, 2002). hFRGN mice displayed higher levels of CDCA, DCA, and CA and their conjugates (Fig. 3B), which are strong FXR/Fxr ligands (Makishima et al., 2002), leading to intestinal Fxr activation and intestinal Fgf15 induction (Fig. 5A). However, hFRGN livers exhibited high CYP7A1 expression (Fig. 4A), suggesting that the signaling pathway associated with Fgf15 appeared to be nonfunctional, as shown by the unchanged ratio of pERK/total ERK (Fig. 5B), suggestive of human hepatocytes and murine intestine miscommunication. Additionally, SHP levels in hFRGN livers (Fig. 3A) were lower, suggesting that high bile acid concentration (Table 5) failed to activate hepatic human FXR to suppress CYP7A1 in hFRGN livers. A plausible explanation attributes this to the bile acid composition changes in hFRGN livers: absence of CDCA and high levels of tβ-MCA (29-fold) and tα-MCA (42-fold) (Table 5), which are FXR antagonists (Sayin et al., 2013). These differential abundances in tMCA and CDCA appear to be the driving forces for decreased hepatic FXR activation in hFRGN livers. High bile acid levels could also induce toxicity by activating nuclear factor-kappa B (NF-κB), which is associated with higher interleukin-6 and COX-2 expression toward enhanced growth and apoptosis resistance in cholangiocarcinoma cells; the release of cytokines can also cause biliary damage (Liu et al., 2014).

High bile acid concentrations in hFRGN bile (Table 5) may lead to gallbladder filling in hFRGN mice (Fig. 1A), in events that are related to bile acid-mediated activation of Tgr5, the transmembrane G-protein-coupled receptor expressed in cholangiocytes and gallbladder epithelial cells (Li et al., 2011; Keitel and Haussinger, 2013; Duboc et al., 2014). Activation of the Tgr5 in gallbladder smooth muscle cells by bile acids, especially lithocholic and deoxycholic acids and their tauroconjugates, would result in smooth muscle cell relaxation, gallbladder filling, and gallbladder stasis (Lavoie et al., 2010; Jones et al., 2015).

Even though high bile acid levels in hFRGN mice were observed, plasma cholesterol level, which is maintained by the low-density lipoproteins (LDL) and high-density lipoproteins (HDL), remained unchanged, whereas liver cholesterol was increased (Table 4). The exact mechanism for these changes is currently unknown. Ellis et al. (2013) reported that LDL, VLDL, and HDL fractions were shifted in chimeric mice, suggesting possible differences of lipid formation and uptake mechanism. Although murine/human 3-hydroxy-3-methylglutaryl-CoA reductase (HMG CoA reductase; which synthesizes cholesterol) levels (Fig. 3A) in hFRGN livers were similar to those in human livers, cholesterol synthesis rates between human and mouse may be different. Certainly, studies are needed to evaluate the upstream pathways of cholesterol synthesis in chimeric livers.

The recent TK-NOG chimeric model may be a better option than hFRGN mice for control of the level of humanization in the mouse liver (Kim et al., 2014). However, the same disrupted signaling between the murine intestine and human hepatocytes and mouse nonparenchymal cells in TK-NOG mouse would also exist. To alleviate elevated bile acids levels, Naugler et al. (2015) suggest that human bile acid production can be controlled by administration of exogenous FGF19 in chimeric mice. However, the dose and dosing regimen of FGF19 administration and the associated effects on drug metabolism and transport are unknown. In addition, the disrupted signaling of human hepatocyte proliferation in the mouse liver requires implantation of human Kupffer cells in mouse liver (Wilson et al., 2014) or exogenous administration of human TGF-β. Certainly, TGF-β and FGF19 are some of the important signaling mechanisms worth investigation for the optimization of humanized mouse liver models.

The distension of the gallbladder, the unchecked hepatocyte proliferation and liver deformity, and miscommunication between liver cell types in the humanized liver and between the mouse intestine and humanized liver, as well as the lack of negative feedback control of the FXR-SHP cascade on bile acid homeostasis (Fig. 7B) would bring about liver toxicity and model instability. These problems will exist not only in the hFRGN mice, but also in other chimeric (humanized) mice such as the PXB and TK-NOG chimeric mice. The dysregulation of bile acid production in h-chimeric mice and physiologic changes that accompany the accumulation of highly toxic bile acids will further contribute to changes in expression of transporter and enzyme in extrahepatic tissues (Fig. 6 and Supplemental Figs. 1 and 2), which would constitute another important consideration in pharmacokinetics and drug disposition studies. Activation of other nuclear receptors, Pxr and Car, owing to elevated bile acids, LCA, and the metabolite 3-keto-5β-cholanic acid (Goodwin and Kliewer, 2002) may result in changes in transporters and enzymes. Bile acids, especially the tMCAs and elevated bilirubin levels in hFRGN livers will further contribute to varying extent of Fxr and Car induction in extrahepatic tissues (Huang et al., 2003; Chen et al., 2011). These translate to induction of targeted transporters and enzymes such as Mrp2, Mrp3, Mrp4 and Mdr1a, Gst4-4, Sult1a1, and Ugt1a1 (Huang et al., 2003; Zollner et al., 2006; Zollner and Trauner, 2009; Wagner et al., 2011) in hFRGN intestine, kidney or brain (Figs. 6 and Supplemental Figs. 1 and 2) and drug dispositional changes. To conclude, instability of the hFRGN liver and extrahepatic tissue with respect to nuclear receptor activation by the dramatic production of differential human (CDCA and CA) and murine (tMCAs) bile acids, both FXR agonists and antagonists, followed by stimulation of the murine intestine and miscommunication among liver cell types and between intestine and humanized liver will induce toxicity and instability issues in this preparation for human drug metabolism studies.

Acknowledgments

The authors thank Dr. Alan F. Hofmann (UCSD) for discussion on bile acid composition in humans, Dr. Carolyn L. Cummins, University of Toronto for communication, and particularly Dr. S.A. Kliewer, Department of Molecular Biology, University of Texas Southwestern Medical Center, for insightful discussions.

Authorship Contributions

Participated in research design: Chow, Evans, Silva, Pang.

Conducted experiments: Chow, Quach, Wang, Pang.

Contributed new reagents or analytic tools: Chow, Quach, Wang, Zhang, Li, Lai, Pang.

Performed data analysis: Chow, Quach, Zhang, Wang, Lai, Pang.

Wrote or contributed to the writing of the manuscript: Chow, Quach, Zhang, Wang, Li, Evans, Silva, Lai, Tirona, Pang.

References

Azuma H, Paulk N, Ranade A, Dorrell C, Al-Dhalimy M, Ellis E, Strom S, Kay MA, Finegold M, and Grompe M (2007) Robust expansion of human hepatocytes in *Fah-/-/Rag2-/-/Il2rg-/-* mice. *Nat Biotechnol* **25**:903–910.

Barnes AJ, Baker DR, Hobby K, Ashton S, Michopoulos F, Spagou K, Loftus NJ, and Wilson ID (2014) Endogenous and xenobiotic metabolite profiling of liver extracts from SCID and chimeric humanized mice following repeated oral administration of troglitazone. *Xenobiotica* **44**:174–185.

Bateman TJ, Reddy VG, Kakuni M, Morikawa Y, and Kumar S (2014) Application of chimeric mice with humanized liver for study of human-specific drug metabolism. *Drug Metab Dispos* **42**:1055–1065.

Chen F, Ma L, Dawson PA, Sinal CJ, Sehayek E, Gonzalez FJ, Breslow J, Ananthanarayanan M, and Shneider BL (2003) Liver receptor homologue-1 mediates species- and cell line-specific bile acid-dependent negative feedback regulation of the apical sodium-dependent bile acid transporter. *J Biol Chem* **278**:19909–19916.

Chen X, Meng Z, Wang X, Zeng S, and Huang W (2011) The nuclear receptor CAR modulates alcohol-induced liver injury. *Lab Invest* **91**:1136–1145.

Cheng L, Tian F, Tian F, Tang L, Chen G, Luo Z, Ren J, and Wang S (2013) Repression of Farnesoid X receptor contributes to biliary injuries of liver grafts through disturbing cholangiocyte bile acid transport. *Am J Transplant* **13**: 3094–3102.

Chiang JY (2003) Bile acid regulation of hepatic physiology: III. Bile acids and nuclear receptors. *Am J Physiol Gastrointest Liver Physiol* **284**:G349–G356.

Chiang JY (2009) Bile acids: regulation of synthesis. *J Lipid Res* **50**:1955–1966.

Chiang JY, Kimmel R, and Stroup D (2001) Regulation of cholesterol 7alpha-hydroxylase gene (CYP7A1) transcription by the liver orphan receptor (LXRalpha). *Gene* **262**:257–265.

Chow EC, Maeng HJ, Liu S, Khan AA, Groothuis GM, and Pang KS (2009) 1α,25-Dihydroxyvitamin $D_{(3)}$ triggered vitamin D receptor and farnesoid X receptor-like effects in rat intestine and liver *in vivo*. *Biopharm Drug Dispos* **30**:457–475.

Chow EC, Magomedova L, Quach HP, Patel R, Durk MR, Fan J, Maeng HJ, Irondi K, Anakk S, Moore DD, et al. (2014) Vitamin D receptor activation down-regulates the small heterodimer partner and increases CYP7A1 to lower cholesterol. *Gastroenterology* **146**:1048–1059.

Chow EC, Wang JZ, Quach HP, Tang H, Evans DC, Li AP, Silva J, and Pang KS (2016) Functional integrity of the chimeric (humanized) mouse liver: enzyme zonation, physiologic spaces, and hepatic enzymes and transporters. *Drug Metab Dispos* **44**:1524–1535.

Cohen J (2014) Toxicology. 'Humanized' mouse detects deadly drug side effects. *Science* **344**:244–245.

De Bleser PJ, Niki T, Rogiers V, and Geerts A (1997) Transforming growth factor-beta gene expression in normal and fibrotic rat liver. *J Hepatol* **26**:886–893.

Delzenne NM, Buc Calderon P, Taper HS, and Roberfroid MB (1992) Comparative hepatotoxicity of cholic acid, deoxycholic acid and lithocholic acid in the rat: in vivo and in vitro studies. *Toxciol Lett* 61:291-304.

De Serres M, Bowers G, Boyle G, Beaumont C, Castellino S, Sigafoos J, Dave M, Roberts A, Shah V, Olson K, et al. (2011) Evaluation of a chimeric (uPA+/+)/SCID mouse model with a humanized liver for prediction of human metabolism. *Xenobiotica* **41**:464–475.

Duboc H, Taché Y, and Hofmann AF (2014) The bile acid TGR5 membrane receptor: from basic research to clinical application. *Dig Liver Dis* **46**:302–312.

Ellis EC, Naugler WE, Parini P, Mörk LM, Jorns C, Zemack H, Sandblom AL, Björkhem I, Ericzon BG, Wilson EM, et al. (2013) Mice with chimeric livers are an improved model for human lipoprotein metabolism. *PLoS One* **8**:e78550.

Emoto C, Yamato Y, Sato Y, Ohshita H, Katoh M, Tateno C, Yokoi T, Yoshizato K, and Iwasaki K (2008) Non-invasive method to detect induction of CYP3A4 in chimeric mice with a humanized liver. *Xenobiotica* **38**:239–248.

Evers R and Chu XY (2008) Role of the murine organic anion-transporting polypeptide 1b2 (Oatp1b2) in drug disposition and hepatotoxicity. *Mol Pharmacol* **74**: 309–311.

Fisher MM and Yousef IM (1973) Sex differences in the bile acid composition of human bile: studies in patients with and without gallstones. *Can Med Assoc J* **109**: 190–193.

Glaser S, Meng F, Han Y, Onori P, Chow BK, Francis H, Venter J, McDaniel K, Marzioni M, Invernizzi P, et al. (2014) Secretin stimulates biliary cell proliferation by regulating expression of microRNA 125b and microRNA let7a in mice. *Gastroenterology* 146:1795–1808.e1712.

Glaser SS and Alpini G (2009) Activation of the cholehepatic shunt as a potential therapy for primary sclerosing cholangitis. *Hepatology* **49**:1795–1797.

Goodwin B and Kliewer SA (2002) Nuclear receptors. I. Nuclear receptors and bile acid homeostasis. *Am J Physiol Gastrointest Liver Physiol* **282**:G926–G931.

Gröer C, Brück S, Lai Y, Paulick A, Busemann A, Heidecke CD, Siegmund W, and Oswald S (2013) LC-MS/MS-based quantification of clinically relevant intestinal uptake and efflux transporter proteins. *J Pharm Biomed Anal* **85**:253–261.

Grompe M and Strom S (2013) Mice with human livers. *Gastroenterology* **145**: 1209–1214.

Handschin C and Meyer UA (2003) Induction of drug metabolism: the role of nuclear receptors. *Pharmacol Rev* **55**:649–673.

Huang W, Zhang J, Chua SS, Qatanani M, Han Y, Granata R, and Moore DD (2003) Induction of bilirubin clearance by the constitutive androstane receptor (CAR). *Proc Natl Acad Sci USA* **100**:4156–4161.

Inagaki T, Choi M, Moschetta A, Peng L, Cummins CL, McDonald JG, Luo G, Jones SA, Goodwin B, Richardson JA, et al. (2005) Fibroblast growth factor 15 functions as an enterohepatic signal to regulate bile acid homeostasis. *Cell Metab* **2**:217–225.

Jaiswal S, Sharma A, Shukla M, Vaghasiya K, Rangaraj N, and Lal J (2014) Novel pre-clinical methodologies for pharmacokinetic drug-drug interaction studies: spotlight on "humanized" animal models. *Drug Metab Rev* **46**:475–493.

Jones H, Alpini G, and Francis H (2015) Bile acid signaling and biliary functions. *Acta Pharm Sin B* **5**:123–128.

Karlgren M, Vildhede A, Norinder U, Wisniewski JR, Kimoto E, Lai Y, Haglund U, and Artursson P (2012) Classification of inhibitors of hepatic organic anion transporting polypeptides (OATPs): influence of protein expression on drug-drug interactions. *J Med Chem* **55**:4740–4763.

Katoh M, Matsui T, Nakajima M, Tateno C, Kataoka M, Soeno Y, Horie T, Iwasaki K, Yoshizato K, and Yokoi T (2004) Expression of human cytochromes P450 in chimeric mice with humanized liver. *Drug Metab Dispos* **32**:1402–1410.

Katoh M, Matsui T, Nakajima M, Tateno C, Soeno Y, Horie T, Iwasaki K, Yoshizato K, and Yokoi T (2005a) *In vivo* induction of human cytochrome P450 enzymes expressed in chimeric mice with humanized liver. *Drug Metab Dispos* **33**:754–763.

Katoh M, Matsui T, Okumura H, Nakajima M, Nishimura M, Naito S, Tateno C, Yoshizato K, and Yokoi T (2005b) Expression of human phase II enzymes in chimeric mice with humanized liver. *Drug Metab Dispos* **33**:1333–1340.

Katoh M, Sawada T, Soeno Y, Nakajima M, Tateno C, Yoshizato K, and Yokoi T (2007) In vivo drug metabolism model for human cytochrome P450 enzyme using chimeric mice with humanized liver. *J Pharm Sci* **96**:428–437.

Katoh M, Watanabe M, Tabata T, Sato Y, Nakajima M, Nishimura M, Naito S, Tateno C, Iwasaki K, Yoshizato K, et al. (2005c) In vivo induction of human cytochrome P450 3A4 by rifabutin in chimeric mice with humanized liver. *Xenobiotica* **35**:863–875.

Keitel V and Häussinger D (2013) TGR5 in cholangiocytes. *Curr Opin Gastroenterol* **29**:299–304.

Kim M, Choi B, Joo SY, Lee H, Lee JH, Lee KW, Lee S, Park JB, Lee SK, and Kim SJ (2014) Generation of humanized liver mouse model by transplant of patient-derived fresh human hepatocytes. *Transplant Proc* **46**:1186–1190.

Kitamura S and Sugihara K (2014) Current status of prediction of drug disposition and toxicity in humans using chimeric mice with humanized liver. *Xenobiotica* **44**: 123–134.

Lavoie B, Balemba OB, Godfrey C, Watson CA, Vassileva G, Corvera CU, Nelson MT, and Mawe GM (2010) Hydrophobic bile salts inhibit gallbladder smooth muscle function via stimulation of GPBAR1 receptors and activation of KATP channels. *J Physiol* **588**:3295–3305.

Lazaridis KN, Pham L, Tietz P, Marinelli RA, deGroen PC, Levine S, Dawson PA, and LaRusso NF (1997) Rat cholangiocytes absorb bile acids at their apical domain via the ileal sodium-dependent bile acid transporter. *J Clin Invest* **100**:2714–2721.

Li N, Nemirovskiy OV, Zhang Y, Yuan H, Mo J, Ji C, Zhang B, Brayman TG, Lepsy C, Heath TG, et al. (2008) Absolute quantification of multidrug resistance-associated protein 2 (MRP2/ABCC2) using liquid chromatography tandem mass spectrometry. *Anal Biochem* **380**:211–222.

Li T, Holmstrom SR, Kir S, Umetani M, Schmidt DR, Kliewer SA, and Mangelsdorf DJ (2011) The G protein-coupled bile acid receptor, TGR5, stimulates gallbladder filling. *Mol Endocrinol* **25**:1066–1071.

Lin BC, Wang M, Blackmore C, and Desnoyers LR (2007) Liver-specific activities of FGF19 require Klotho beta. *J Biol Chem* **282**:27277–27284.

Liu L, Halladay JS, Shin Y, Wong S, Coraggio M, La H, Baumgardner M, Le H, Gopaul S, Boggs J, et al. (2011) Significant species difference in amide hydrolysis of GDC-0834, a novel potent and selective Bruton's tyrosine kinase inhibitor. *Drug Metab Dispos* **39**:1840–1849.

Liu R, Zhao R, Zhou X, Liang X, Campbell DJ, Zhang X, Zhang L, Shi R, Wang G, Pandak WM, et al. (2014) Conjugated bile acids promote cholangiocarcinoma cell invasive growth through activation of sphingosine 1-phosphate receptor 2. *Hepatology* **60**:908–918.

Makishima M (2005) Nuclear receptors as targets for drug development: regulation of cholesterol and bile acid metabolism by nuclear receptors. *J Pharmacol Sci* **97**: 177–183.

Makishima M, Lu TT, Xie W, Whitfield GK, Domoto H, Evans RM, Haussler MR, and Mangelsdorf DJ (2002) Vitamin D receptor as an intestinal bile acid sensor. *Science* **296**:1313–1316.

Maroni L, Haibo B, Ray D, Zhou T, Wan Y, Meng F, Marzioni M, and Alpini G (2015) Functional and structural features of cholangiocytes in health and disease. *Cell Mol Gastroenterol Hepatol* **1**:368–380.

Meng F, Onori P, Hargrove L, Han Y, Kennedy L, Graf A, Hodges K, Ueno Y, Francis T, Gaudio E, et al. (2014) Regulation of the histamine/VEGF axis by miR-125b during cholestatic liver injury in mice. *Am J Pathol* **184**:662–673.

Naud J, Michaud J, Boisvert C, Desbiens K, Leblond FA, Mitchell A, Jones C, Bonnardeaux A, and Pichette V (2007) Down-regulation of intestinal drug transporters in chronic renal failure in rats. *J Pharmacol Exp Ther* **320**:978–985.

Naud J, Michaud J, Leblond FA, Lefrancois S, Bonnardeaux A, and Pichette V (2008) Effects of chronic renal failure on liver drug transporters. *Drug Metab Dispos* **36**: 124–128.

Naugler WE, Tarlow BD, Fedorov LM, Taylor M, Pelz C, Li B, Darnell J, and Grompe M (2015) Fibroblast growth factor signaling controls liver size in mice with humanized livers. *Gastroenterology* **149**:728–40.e15.

Nishimura M, Yoshitsugu H, Yokoi T, Tateno C, Kataoka M, Horie T, Yoshizato K, and Naito S (2005) Evaluation of mRNA expression of human drug-metabolizing enzymes and transporters in chimeric mouse with humanized liver. *Xenobiotica* **35**: 877–890.

Ohtsuki S, Kawakami H, Inoue T, Nakamura K, Tateno C, Katsukura Y, Obuchi W, Uchida Y, Kamiie J, Horie T, et al. (2014) Validation of uPA/SCID mouse with humanized liver as a human liver model: protein quantification of transporters, cytochromes P450, and UDP-glucuronosyltransferases by LC-MS/MS. *Drug Metab Dispos* **42**:1039–1043.

Okumura H, Katoh M, Sawada T, Nakajima M, Soeno Y, Yabuuchi H, Ikeda T, Tateno C, Yoshizato K, and Yokoi T (2007) Humanization of excretory pathway in chimeric mice with humanized liver. *Toxicol Sci* **97**:533–538.

Omenetti A, Syn WK, Jung Y, Francis H, Porrello A, Witek RP, Choi SS, Yang L, Mayo MJ, Gershwin ME, et al. (2009) Repair-related activation of hedgehog signaling promotes cholangiocyte chemokine production. *Hepatology* **50**:518–527.
Qiu X, Bi YA, Balogh LM, and Lai Y (2013) Absolute measurement of species differences in sodium taurocholate cotransporting polypeptide (NTCP/Ntcp) and its modulation in cultured hepatocytes. *J Pharm Sci* **102**:3252–3263.
Reich M, Deutschmann K, Sommerfeld A, Klindt C, Kluge S, Kubitz R, Ullmer C, Knoefel WT, Herebian D, Mayatepek E, et al. (2016) TGR5 is essential for bile acid-dependent cholangiocyte proliferation in vivo and in vitro. *Gut* **65**:487–501.
Rossi SS, Converse JL, and Hofmann AF (1987) High pressure liquid chromatographic analysis of conjugated bile acids in human bile: simultaneous resolution of sulfated and unsulfated lithocholyl amidates and the common conjugated bile acids. *J Lipid Res* **28**:589–595.
Samuelsson K, Pickup K, Sarda S, Foster JR, Randall K, Abrahamsson A, Jacobsen M, Weidolf L, and Wilson I (2014) Troglitazone metabolism and transporter effects in chimeric mice: a comparison between chimeric humanized and chimeric murinized FRG mice. *Xenobiotica* **44**:186–195.
Sanoh S, Horiguchi A, Sugihara K, Kotake Y, Tayama Y, Uramaru N, Ohshita H, Tateno C, Horie T, Kitamura S, et al. (2012) Predictability of metabolism of ibuprofen and naproxen using chimeric mice with human hepatocytes. *Drug Metab Dispos* **40**:2267–2272.
Sanoh S and Ohta S (2014) Chimeric mice transplanted with human hepatocytes as a model for prediction of human drug metabolism and pharmacokinetics. *Biopharm Drug Dispos* **35**:71–86.
Sayin SI, Wahlström A, Felin J, Jäntti S, Marschall HU, Bamberg K, Angelin B, Hyötyläinen T, Orešič M, and Bäckhed F (2013) Gut microbiota regulates bile acid metabolism by reducing the levels of tauro-beta-muricholic acid, a naturally occurring FXR antagonist. *Cell Metab* **17**:225–235.
Schon HT and Weiskirchen R (2014) Immunomodulatory effects of transforming growth factor-β in the liver. *Hepatobiliary Surg Nutr* **3**:386–406.
Sinha J, Chen F, Miloh T, Burns RC, Yu Z, and Shneider BL (2008) beta-Klotho and FGF-15/19 inhibit the apical sodium-dependent bile acid transporter in enterocytes and cholangiocytes. *Am J Physiol Gastrointest Liver Physiol* **295**:G996–G1003.
Strom SC, Davila J, and Grompe M (2010) Chimeric mice with humanized liver: tools for the study of drug metabolism, excretion, and toxicity. *Methods Mol Biol* **640**: 491–509.
Takahashi S, Fukami T, Masuo Y, Brocker CN, Xie C, Krausz KW, Wolf CR, Henderson CJ, and Gonzalez FJ (2016) Cyp2c70 is responsible for the species difference in bile acid metabolism between mice and humans. *J Lipid Res* **57**:2130–2137.
Tateno C, Yoshizane Y, Saito N, Kataoka M, Utoh R, Yamasaki C, Tachibana A, Soeno Y, Asahina K, Hino H, et al. (2004) Near completely humanized liver in mice shows human-type metabolic responses to drugs. *Am J Pathol* **165**:901–912.
Vildhede A, Karlgren M, Svedberg EK, Wisniewski JR, Lai Y, Norén A, and Artursson P (2014) Hepatic uptake of atorvastatin: influence of variability in transporter expression on uptake clearance and drug-drug interactions. *Drug Metab Dispos* **42**:1210–1218.
Wagner M, Zollner G, and Trauner M (2011) Nuclear receptors in liver disease. *Hepatology* **53**:1023–1034.
Wahlström A, Sayin SI, Marschall HU, and Bäckhed F (2016) Intestinal crosstalk between bile acids and microbiota and its impact on host metabolism. *Cell Metab* **24**:41–50.
Weiskirchen R and Tacke F (2014) Cellular and molecular functions of hepatic stellate cells in inflammatory responses and liver immunology. *Hepatobiliary Surg Nutr* **3**:344–363.
Wilson EM, Bial J, Tarlow B, Bial G, Jensen B, Greiner DL, Brehm MA, and Grompe M (2014) Extensive double humanization of both liver and hematopoiesis in FRGN mice. *Stem Cell Res (Amst)* **13** (3 Pt A):404–412.
Xia X, Francis H, Glaser S, Alpini G, and LeSage G (2006) Bile acid interactions with cholangiocytes. *World J Gastroenterol* **12**:3553–3563.
Xu D, Nishimura T, Nishimura S, Zhang H, Zheng M, Guo YY, Masek M, Michie SA, Glenn J, and Peltz G (2014) Fialuridine induces acute liver failure in chimeric TK-NOG mice: a model for detecting hepatic drug toxicity prior to human testing. *PLoS Med* **11**:e1001628.
Xu D, Wu M, Nishimura S, Nishimura T, Michie SA, Zheng M, Yang Z, Yates AJ, Day JS, Hillgren KM, et al. (2015) Chimeric TK-NOG mice: a predictive model for cholestatic human liver toxicity. *J Pharmacol Exp Ther* **352**:274–280.
Yoshizato K, Tateno C, and Utoh R (2012) Mice with liver composed of human hepatocytes as an animal model for drug testing. *Curr Drug Discov Technol* **9**:63–76.
Zollner G, Marschall HU, Wagner M, and Trauner M (2006) Role of nuclear receptors in the adaptive response to bile acids and cholestasis: pathogenetic and therapeutic considerations. *Mol Pharm* **3**:231–251.
Zollner G and Trauner M (2009) Nuclear receptors as therapeutic targets in cholestatic liver diseases. *Br J Pharmacol* **156**:7–27.

Address correspondence to: Dr. K. Sandy Pang, Leslie Dan Faculty of Pharmacy, University of Toronto, 144 College Street, Toronto, Ontario, Canada M5S 3M2. E-mail: ks.pang@utoronto.ca